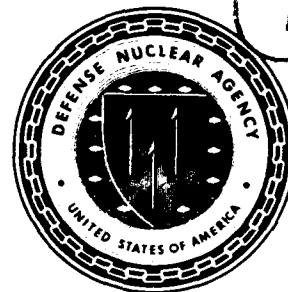


**AD-A248 174**



**Defense Nuclear Agency  
Alexandria, VA 22310-3398**



**DNA-TR-91-99**

## **Fast Electrochromic Switching for Optical Hardening Applications**

**Stuart F. Cogan, et al.  
EIC Laboratories, Inc.  
111 Downey Street  
Norwood, MA 02062**



**April 1992**

**Technical Report**

**CONTRACT No. DNA 001-88-C-0102**

**Approved for public release;  
distribution is unlimited.**

**92-08401**



Destroy this report when it is no longer needed. Do not return to sender.

PLEASE NOTIFY THE DEFENSE NUCLEAR AGENCY,  
ATTN: CSTI, 6801 TELEGRAPH ROAD, ALEXANDRIA, VA  
22310-3398, IF YOUR ADDRESS IS INCORRECT, IF YOU  
WISH IT DELETED FROM THE DISTRIBUTION LIST, OR  
IF THE ADDRESSEE IS NO LONGER EMPLOYED BY YOUR  
ORGANIZATION.



## DISTRIBUTION LIST UPDATE

This mailer is provided to enable DNA to maintain current distribution lists for reports. We would appreciate your providing the requested information.

- ☐ Add the individual listed to your distribution list.
- ☐ Delete the cited organization/individual.
- ☐ Change of address.

**NOTE:**  
Please return the mailing label from the document so that any additions, changes, corrections or deletions can be made more easily.

NAME: \_\_\_\_\_

ORGANIZATION: \_\_\_\_\_

### OLD ADDRESS

### CURRENT ADDRESS

\_\_\_\_\_  
\_\_\_\_\_  
\_\_\_\_\_

\_\_\_\_\_  
\_\_\_\_\_  
\_\_\_\_\_

TELEPHONE NUMBER: (    ) \_\_\_\_\_

SUBJECT AREA(s) OF INTEREST:

\_\_\_\_\_  
\_\_\_\_\_  
\_\_\_\_\_

\_\_\_\_\_  
\_\_\_\_\_  
\_\_\_\_\_

DNA OR OTHER GOVERNMENT CONTRACT NUMBER: \_\_\_\_\_

CERTIFICATION OF NEED-TO-KNOW BY GOVERNMENT SPONSOR (if other than DNA):

SPONSORING ORGANIZATION: \_\_\_\_\_

CONTRACTING OFFICER OR REPRESENTATIVE: \_\_\_\_\_

SIGNATURE: \_\_\_\_\_

CUT HERE AND RETURN



•  
•

Director  
Defense Nuclear Agency  
ATTN: TITL  
Washington, DC 20305-1000

•  
•

Director  
Defense Nuclear Agency  
ATTN: TITL  
Washington, DC 20305-1000

REPORT DOCUMENTATION PAGE			Form Approved OMB No. 0704-0188	
Public reporting burden for this collection of information is estimated to average 1 hour per response, including the time for reviewing instructions, searching existing data sources, gathering and maintaining the data needed, and completing and reviewing the collection of information. Send comments regarding this burden estimate or any other aspect of this collection of information, including suggestions for reducing this burden, to Washington Headquarters Services, Directorate for Information Operations and Reports, 1215 Jefferson Davis Highway, Suite 1204, Arlington, VA 22202-4302, and to the Office of Management and Budget, Paperwork Reduction Project (0704-0188), Washington, DC 20503				
1. AGENCY USE ONLY (Leave blank)	2. REPORT DATE 920401	3. REPORT TYPE AND DATFS COVERED Technical - 880805-901205		
4. TITLE AND SUBTITLE Fast Electrochromic Switching for Optical Hardening Applications		5. FUNDING NUMBERS C - DNA 001-88-C-0102 PE - 63224C PR - SF TA - SB WU - DH050600		
6. AUTHOR(S) Stuart F. Cogan, R. David Rauh, Trung H. Nguyen, Rochelle B. Jones, John D. Westwood, and Louis L. Wu				
7. PERFORMING ORGANIZATION NAME(S) AND ADDRESS(ES) EIC Laboratories, Inc. 111 Downey Street Norwood, MA 02062		8. PERFORMING ORGANIZATION REPORT NUMBER  C946F		
9. SPONSORING/MONITORING AGENCY NAME(S) AND ADDRESS(ES) Defense Nuclear Agency 6801 Telegraph Road Alexandria, VA 22310-3398 RAEV/Meisenhelder		10. SPONSORING/MONITORING AGENCY REPORT NUMBER  DNA-TR-91-99		
11. SUPPLEMENTARY NOTES This work was sponsored by the Defense Nuclear Agency under RDT&E RMC Code B7664 D SF SB 00002 PRPD 1950A 25904D.				
12a. DISTRIBUTION/AVAILABILITY STATEMENT  Approved for public release; distribution is unlimited.			12b. DISTRIBUTION CODE	
13. ABSTRACT (Maximum 200 words)  Infrared optical switching devices based on closed-tube-vapor-transport grown single crystals of group IV metal dichalcogenides were investigated. Reversible infrared reflectance modulation was identified in alkali metal intercalated HfS <sub>2</sub> and ZrS <sub>2</sub> . A reflectance driven transmittance modulation of 0.01% to 50% from 2-16 μm was observed with Li <sub>2</sub> HfS <sub>2</sub> single crystals chemically lithiated and delithiated. Similar, although less dramatic, modulation was obtained with Ag <sub>2</sub> HfS <sub>2</sub> crystals.  Efforts to develop practical optical switching devices based on this IR modulation focused on the incorporation of electroactive and photoactive electron donor-acceptor complexes in the van der Waals' gaps of the crystals. Electron donor (e.g., Li or Ag) intercalation is readily achieved because of coulombic stabilization of the intercalated crystal through intercalation of the chalcogens (e.g., S) and the donor cation. Intercalation of electron acceptors (e.g., I and Br) into reduced (donor intercalated) dichalcogenides was found energetically unfavorable and resulted in deintercalation of the donor. Mixed-metal (group IV and V) dichalcogenide crystals, that are intrinsically n-type, were also used as hosts for acceptor intercalation. The as-grown mixed-metal crystals had higher				
14. SUBJECT TERMS Optical Hardening Dichalcogenides Crystal Growth Intercalation			15. NUMBER OF PAGES 52	
			16. PRICE CODE	
17. SECURITY CLASSIFICATION OF REPORT UNCLASSIFIED	18. SECURITY CLASSIFICATION OF THIS PAGE UNCLASSIFIED	19. SECURITY CLASSIFICATION OF ABSTRACT UNCLASSIFIED	20. LIMITATION OF ABSTRACT SAR	

CLASSIFIED BY:

N/A since Unclassified.

DECLASSIFY ON:

N/A since Unclassified.

## 9. Sponsoring/Monitoring Agency Name(s) and Address(es) (Continued):

Director  
Strategic Defense Initiative Organization  
Pentagon  
Washington, D.C. 20301-7100

## 11. Supplementary Notes (Continued)

Additional support and funding provided by the Strategic Defense Initiative Organization.

## 13. Abstract (Continued)

electrical conductivities and were more IR reflective than pure  $\text{HfS}_2$  or  $\text{ZrS}_2$ . Attempts to intercalate I and Br into the mixed-metal crystals resulted in extensive exfoliation. The use of metallocenes, principally chromocene, to create a  $5\text{\AA}$  c-axis expansion was successful and led to the preparation of  $\text{I}_2$  "intercalated" chromocene- $\text{HfS}_2$ . The nature of the bonding between the intercalated  $\text{I}_2$  and both the chromocene and  $\text{HfS}_2$  remains unknown. ✓

Electrically driven optical switching in the 700-1100 nm wavelength range was observed in  $\text{HfS}_2$  crystals that had been lithiated and treated in iodine. A sharp increase in electrical conductivity and decrease in transmittance was observed at electrical field strengths of  $0.7\text{ V}/\mu\text{m}$  in the c-axis direction. The switching was reversible with applied electric field and independent of polarity.

Accession For	
NTIS CRA&I	<input checked="" type="checkbox"/>
DTIC TAB	<input type="checkbox"/>
Unannounced	<input type="checkbox"/>
Justification	
By	
Distribution /	
Availability Codes	
Dist	Availability / or Special
A-1	



## SUMMARY

The objective of the program was the development of rapid switching optical shutters. The shutters were intended for optical hardening of space and ground-based SDI sensors against hostile laser weapons and high intensity flashes from conventional and nuclear weapons. Such protection would also be valuable for other military components, such as targeting and surveillance sensors, night vision devices, and tracking and imaging optics.

The principal innovation of the program was the incorporation of photoactive and electroactive electron donor-acceptor complexes into the van der Waals' gaps of group IV metal dichalcogenides. In response to an external electrical field, the donor-acceptor complexes should ionize and promote an electron to the conduction band of the host crystal. The increase in the density of free electrons causes the crystal to switch from its original transmissive state to a reflective state.

The metal dichalcogenides  $\text{HfS}_2$ ,  $\text{ZrS}_2$ ,  $\text{SnS}_2$ , and  $\text{CdI}_2$  were successfully grown by a closed-tube-vapor-transport technique. Reversible infrared reflectance modulation was identified in alkali metal intercalated  $\text{HfS}_2$  and  $\text{ZrS}_2$ . A reflectance driven transmittance modulation of 0.01% to 50% from 2-16  $\mu\text{m}$  was observed with  $\text{Li}_x\text{HfS}_2$  single crystals chemically lithiated and delithiated. Similar, although less dramatic, modulation was obtained with  $\text{Ag}_x\text{HfS}_2$  crystals.

Efforts to develop practical optical switching devices based on this IR modulation focused on the incorporation of electron donor-acceptor complexes in the van der Waals' gaps of the crystals. Electron donor (e.g., Li or Ag) intercalation was readily achieved. Intercalation of electron acceptors, principally I and Br into reduced (donor intercalated) dichalcogenides, however, was found energetically unfavorable and resulted in deintercalation of the donor. Mixed-metal (group IV and V) dichalcogenide crystals, that are intrinsically n-type, were also used as hosts for acceptor intercalation. The as-grown mixed-metal crystals had higher electrical conductivities and were more IR reflective than pure  $\text{HfS}_2$  or  $\text{ZrS}_2$ . Attempts to intercalate I and Br into the mixed-metal crystals resulted in extensive exfoliation of the crystals. The use of metallocenes, principally chromocene, to create a 5Å c-axis expansion was successful and led to the preparation of  $\text{I}_2$  "intercalated" chromocene- $\text{HfS}_2$ . The nature of the bonding between the intercalated  $\text{I}_2$  and both the chromocene and  $\text{HfS}_2$  remains unknown.

Electrically driven optical switching in the 700-1100 nm wavelength range was observed in  $\text{HfS}_2$  crystals that had been lithiated and treated in iodine. A sharp increase in electrical conductivity and decrease in transmittance was observed at electrical field strengths of approximately 0.7 V/ $\mu\text{m}$  in the c-axis direction. The observed switching was fully reversible and did not depend on the polarity of the applied voltage. This current-voltage behavior of the switching in intercalated crystals was different from that reported for "electroformed"  $\text{SnS}_2$  or  $\text{HfS}_2$ .

The major difficulty encountered in the program was the unsuitability of the dichalcogenide crystals as hosts for electron acceptors even in the presence of intercalated electron donors or in crystals grown directly with mixed group IV and V metals. The use of bulky electron donors to increase the van der Waals' spacing was successful in promoting some form of iodine intercalation but the electrical and optical characteristics of these crystals remain to be determined. Besides the dichalcogenides, other layered materials that are amphoteric (have both acid and base properties) and intercalate both electron donors or acceptors directly would have potential as a guest for electron donor-acceptor complexes. Graphite is the best example of such a material.

## TABLE OF CONTENTS

Section	Page
SUMMARY .....	iii
LIST OF ILLUSTRATIONS .....	v
LIST OF TABLES .....	vi
1 INTRODUCTION .....	1
2 CRYSTAL GROWTH .....	2
3 HfS <sub>2</sub> POWDER PREPARATION .....	6
4 INTERCALATION OF CHARGE TRANSFER COMPLEXES .....	7
4.1 AgI in HfS <sub>2</sub> .....	7
4.2 Intercalation of Ag and I <sub>2</sub> into HfS <sub>2</sub> Single Crystals .....	12
5 MIXED-METAL DICHALCOGENIDES .....	15
5.1 Growth and Characterization of Mixed-Metal Crystals .....	15
5.2 Halide Intercalation .....	16
6 METALLOCENE INTERCALATION .....	20
6.1 Metallocene - I <sub>2</sub> Intercalation .....	24
7 CONCLUSION .....	29
8 LIST OF REFERENCES .....	30
APPENDIX	
A OPTICAL CHARACTERIZATION OF SINGLE CRYSTAL HfS <sub>2</sub> AND ZrS <sub>2</sub> .....	31
B ORGANIC BASE INTERCALATION .....	41

## LIST OF ILLUSTRATIONS

Figure		Page
1	Temperature profile for the growth of $ZrS_2$ crystals .....	3
2	Time-temperature sequence for CTVT growth of $HfS_2$ crystals .....	4
3	Time-temperature sequence for CTVT growth of $ZrS_2$ crystals .....	4
4	Time-temperature sequence for CTVT growth of $SnS_2$ crystals .....	5
5	Time-temperature sequence for CTVT growth of $CdI_2$ crystals .....	5
6	Temperature profile for preparation of $HfS_2$ "crystal-powder" .....	6
7	EDS spectrum of as-grown $HfS_2$ crystal-powder .....	9
8	EDS spectrum of $HfS_2$ crystal powder showing the presence of Ag in the $HfS_2$ following a $750^\circ C$ diffusion anneal with Ag powder .....	9
9	EDS spectrum of $Ag_xHfS_2$ powder following a $400^\circ C$ treatment in $I_2$ .....	10
10	DSC spectra of $Ag_xHfS_2$ crystal powder following treatment in $I_2$ .....	10
11	DSC spectrum of as-grown $HfS_2$ crystal powder .....	11
12	Thermogravimetric analysis of $HfS_2$ , $Ag_xHfS_2$ , and $Ag_xHfS_2(I_2 \text{ treated})$	11
13	Thermogravimetric analysis of $AgI$ and $Ag_xHfS_2(I_2)$ for $x = 0.1, 0.3,$ and $0.5$ .....	12
14	Infrared transmittance of a $HfS_2$ single crystal following successive Ag intercalation and treatment with $I_2$ .....	14
15	Scanning electron micrograph of a partially exfoliated $Hf_{0.9}Nb_{0.1}S_2$ crystal after heat treatment in $I_2$ at $300^\circ C$ .....	19
16	EDS spectrum of $HfS_2$ following cobaltocene intercalation .....	23
17	EDS spectrum of $HfS_2$ following chromocene intercalation.....	23
18	EDS spectrum of as-grown $HfS_2$ crystal powder .....	24
19	EDS spectrum of $HfS_2$ following cobaltocene intercalation and $I_2$ treatment .....	25
20	EDS spectrum of $HfS_2$ following chromocene intercalation and $I_2$ treatment .....	25

## LIST OF ILLUSTRATIONS (Continued)

Figure		Page
21	TGA spectrum of chromocene intercalated $\text{HfS}_2$ following heat treatment in $\text{I}_2$ .....	27
22	TGA spectrum of cobaltocene intercalated $\text{HfS}_2$ (3 days at $300^\circ\text{C}$ ) following heat treatment in $\text{I}_2$ .....	27
23	TGA spectrum of cobaltocene intercalated $\text{HfS}_2$ (5 days at $300^\circ\text{C}$ ) following heat treatment in $\text{I}_2$ .....	28
24	Hemispherical reflectance of an as-grown $\text{ZrS}_2$ crystal .....	32
25	Hemispherical reflectance of an as-grown $\text{HfS}_2$ single crystal with a thickness of $15\ \mu\text{m}$ .....	32
26	Transmittance of the same $\text{HfS}_2$ single crystal as in Figure 25 .....	33
27	Absorbance spectra in the near infrared of single crystal $\text{HfS}_2$ during lithium intercalation to the composition $\text{LiHfS}_2$ .....	34
28	Absorbance spectra in the near infrared of single crystal $\text{ZrS}_2$ during the initial stages of lithium intercalation (see text) .....	35
29	Absorbance of a $\text{HfS}_2$ single crystal from 350-800 nm during immersion in 2.2M n-butyllithium in hexane .....	36
30	Hemispherical reflectance of an as-grown $\text{SnS}_2$ crystal from 2-16 $\mu\text{m}$ ....	37
31	Transmittance of an as-grown $\text{SnS}_2$ crystal from 2-16 $\mu\text{m}$ .....	37
32	Absorbance of a $\text{SnS}_2$ single crystal from 350-800 nm during immersion in 1.1M n-butyllithium in hexane .....	38
33	Absorbance of a $\text{SnS}_2$ single crystal from 675-1650 nm during immersion in 1.1M n-butyllithium in hexane .....	38
34	Hemispherical reflectance of an as-grown $\text{CdI}_2$ crystal from 2-16 $\mu\text{m}$ .....	40
35	Transmittance of an as-grown $\text{CdI}_2$ crystal from 2-16 $\mu\text{m}$ .....	40

## LIST OF TABLES

Table		Page
1	CTVT growth conditions for the dichalcogenide crystals investigated ....	3
2	X-ray data for $\text{HfS}_2$ crystal powder and Ag intercalated powder .....	8
3	AgI stoichiometry from TGA results .....	12
4	van der Pauw electrical resistivity parallel to the c-axis of $\text{Ag}_x\text{HfS}_2$ .....	14
5	Compilation of data on mixed-metal dichalcogenide crystals as-grown and after treatment in $\text{I}_2$ vapor .....	16
6	$\text{HfS}_2$ before and after intercalation experiments.....	17
7	$\text{Hf}_{0.9}\text{V}_{0.1}\text{S}_2$ before and after $\text{I}_2$ intercalation experiments .....	17
8	$\text{Hf}_{0.9}\text{Nb}_{0.1}\text{S}_2$ before and after $\text{I}_2$ intercalation experiments .....	18
9	$\text{Hf}_{0.9}\text{Ta}_{0.1}\text{S}_2$ before and after $\text{I}_2$ intercalation experiments.....	18
10	$\text{Hf}_{0.7}\text{V}_{0.3}\text{S}_2$ before and after $\text{I}_2$ intercalation experiments .....	18
11	$\text{HfS}_2$ before and after ferrocene intercalation .....	21
12	$\text{ZrS}_2$ before and after ferrocene intercalation .....	21
13	$\text{HfS}_2$ single crystal powder with metallocene intercalation.....	22
14	Metallocene and $\text{I}_2$ intercalation into $\text{HfS}_2$ single crystal powder .....	26

## SECTION 1

### INTRODUCTION

The objective of the program was the development of rapid switching optical devices based on metal dichalcogenide single crystals. We have proposed to develop devices that are capable of transmissive to reflective modulation over a broad range of wavelengths in the thermal infrared, near infrared, and visible regions. The proposed devices were based on single crystals of  $\text{HfS}_2$ ,  $\text{ZrS}_2$ ,  $\text{SnS}_2$ , and  $\text{CdI}_2$ . These compounds have a layered structure comprised of trilayers of chalcogen-metal-chalcogen planes of atoms in which the metal cation is octahedrally coordinated with six chalcogenide anions. While the metal-chalcogen bonding within the layers is predominantly covalent, the trilayers interact only weak through van der Waals' bonding. The layered structure permits intercalation of a large number of molecules into the van der Waals' gaps. The objective of the program was to intercalate electrically and optically ionizable reduction/oxidation (redox) couples into the van der Waals' gap of the crystals. In response to an external electric field or high intensity illumination, the redox couples ionize and promote electrons to the conduction band of the host crystal. The increase in the density of the free electrons causes the crystal to switch from its original transmissive state to a reflective state.

The body of this report describes the major task of the program which was the preparation and characterization of dichalcogenide crystals with charge transfer complexes intercalated in their van der Waals' gaps. Related work involving the optical characterization of lithium intercalated single crystals and the use of basic (electron donating) organic molecules to expand the van der Waals' gaps of the crystals is included in Appendices A and B, respectively.

## SECTION 2

### CRYSTAL GROWTH

Dichalcogenide single crystals were grown by closed-tube-vapor transport (CTVT) using iodine as the chemical transport agent (1,2). The starting materials were stoichiometric quantities of high purity hafnium or zirconium powder and resublimed sulfur. Crystal growth was carried out in 25 cm by 2.2 cm ID quartz tubes that were washed and etched with 49% hydrofluoric acid, rinsed with distilled water, and then dried at mildly elevated temperatures ( $\sim 105^\circ\text{C}$ ). Iodine was added at a concentration of  $5\text{ mg/cm}^3$  of tube volume. With the reactant end cooled in liquid nitrogen to prevent sublimation of iodine, the tube was evacuated with a liquid nitrogen trapped diffusion pump to a pressure of  $\sim 10\text{ mPa}$  ( $10^{-4}$  torr) and sealed. A microprocessor-controlled, three-zone furnace was used for crystal growth. Starting reagents that had adhered to the tube wall were back-transported to the reactant zone by heating the growth and reactant zones to  $950^\circ\text{C}$  and  $900^\circ\text{C}$ , respectively, for eight hours. The growth zone temperature was then reduced at a rate of  $<1.4^\circ\text{C/hr}$  to  $815^\circ\text{C}$  for  $\text{HfS}_2$  and  $825^\circ\text{C}$  for  $\text{ZrS}_2$ . Growth times were 96 hr for  $\text{HfS}_2$  and 76 hr for  $\text{ZrS}_2$ .

Typically, 50 mg of highly oriented plate-like crystals having specular surfaces were obtained in each growth run. The size and thickness of the crystals varied greatly. Most crystals had a basal plane area of approximately  $0.5\text{ cm}^2$  and a thickness between 5 and  $30\text{ }\mu\text{m}$ . Occasionally, large crystals with basal plane areas of  $3\text{ cm}^2$  were obtained. A stoichiometric ratio 2.00 for sulfur to hafnium was calculated from the weight change after calcining  $\text{HfS}_2$  crystals in air at  $750^\circ\text{C}$  for 80 hr.

In addition to  $\text{HfS}_2$  and  $\text{ZrS}_2$ , crystals of  $\text{SnS}_2$  and  $\text{CdI}_2$  were also grown by the CTVT method. Both  $\text{SnS}_2$  and  $\text{CdI}_2$  crystals with basal plane areas of  $\sim 2\text{ cm}^2$  and thickness of  $10\text{--}100\text{ }\mu\text{m}$  for  $\text{SnS}_2$  and  $15\text{--}40\text{ }\mu\text{m}$  for  $\text{CdI}_2$  were obtained. The growth conditions for the four dichalcogenides investigated are summarized in Table 1.

In order to grow crystals of high quality, great care was necessary in controlling the temperature of the furnace. To achieve the desired temperature profile, each zone of the furnace was independently controlled and programmed. Figure 1 shows the temperature profile for  $\text{ZrS}_2$  growth. Crystal growth occurs over a 4 cm band with the zone of fastest growth displaced about 3 cm from the growth zone center towards the reactant zone. The time-temperature sequences for the growth of the  $\text{HfS}_2$ ,  $\text{ZrS}_2$ ,  $\text{SnS}_2$ , and  $\text{CdI}_2$  crystals are summarized in Figures 2-5, respectively.

Table 1. CTVT growth conditions for the dichalcogenide crystals investigated.

Dichalcogenide	Reactant Zone (°C)	Growth Zone (°C)	Growth Time (hr)
HfS <sub>2</sub>	895	815	96
ZrS <sub>2</sub>	900	825	72
SnS <sub>2</sub>	700	620	36
CdI <sub>2</sub>	370	310	39

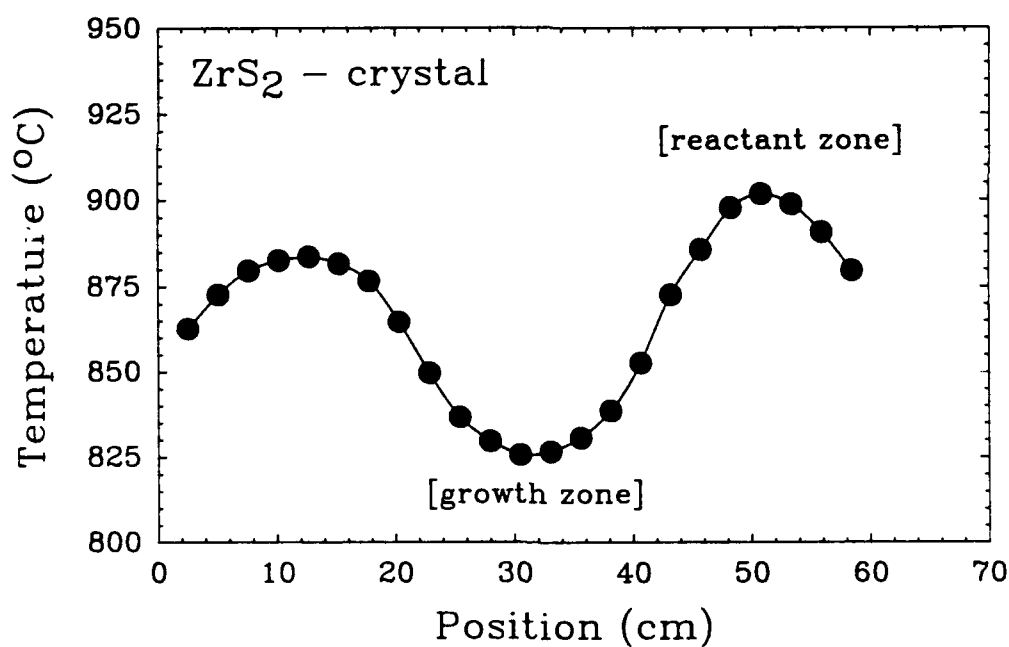


Figure 1. Temperature profile for the growth of ZrS<sub>2</sub> crystals.

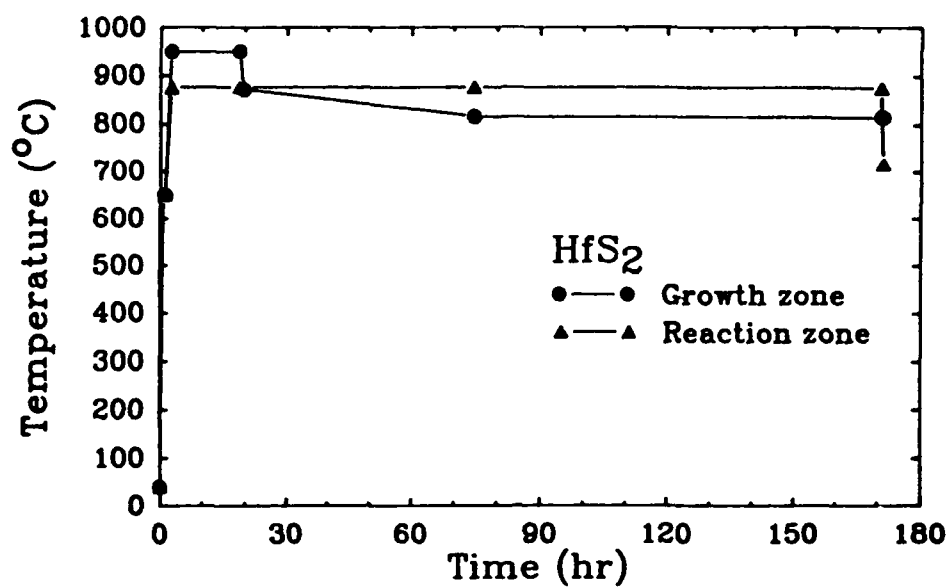


Figure 2. Time-temperature sequence for CTVT growth of HfS<sub>2</sub> crystals.

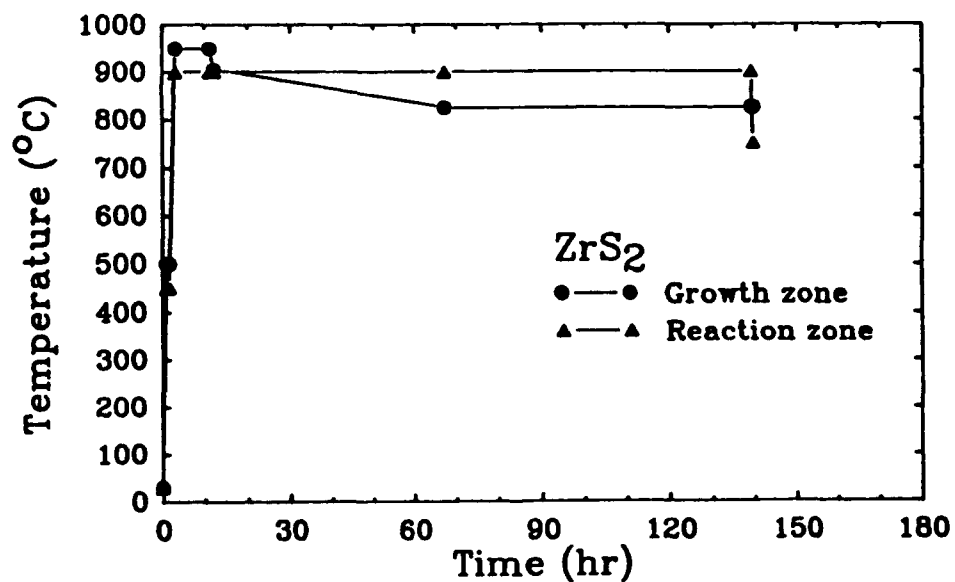


Figure 3. Time-temperature sequence for CTVT growth of ZrS<sub>2</sub> crystals.

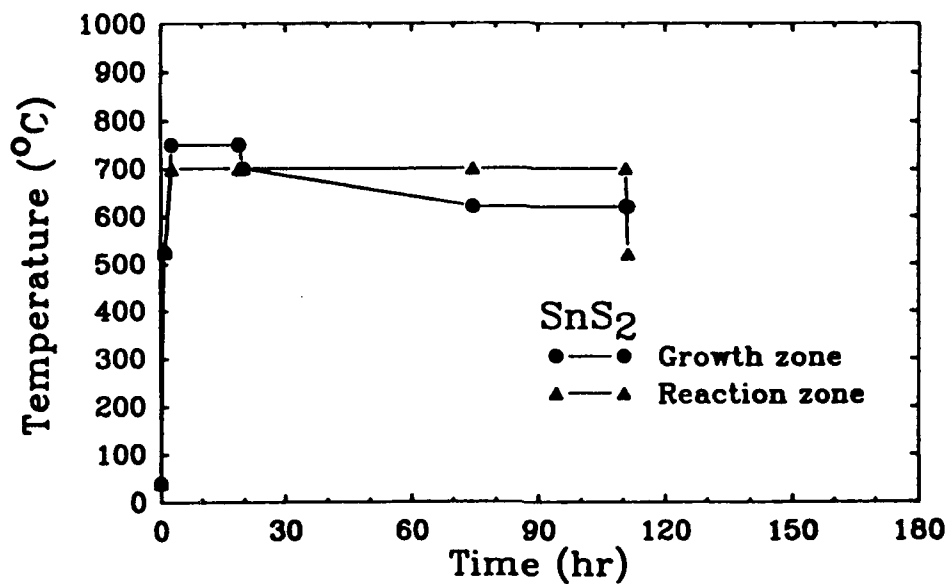


Figure 4. Time-temperature sequence for CTVT growth of SnS<sub>2</sub> crystals.

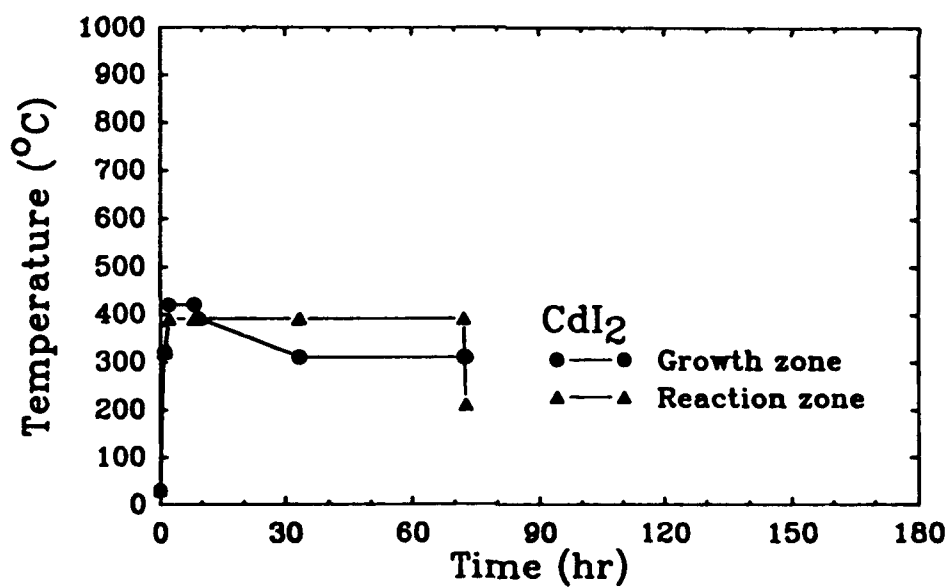


Figure 5. Time-temperature sequence for CTVT growth of CdI<sub>2</sub> crystals.

### SECTION 3

#### HfS<sub>2</sub> POWDER PREPARATION

Due to the lack of a readily available source, high quality HfS<sub>2</sub> powder was produced in-house by growing a large number of small crystals with the CTVT method and then grinding them into powder. The crystal growth for powder preparation was carried out in a 13 cm ID 3-zone tube furnace with the temperature profile shown in Figure 6. X-ray diffraction of the "crystal powder" indicated single phase HfS<sub>2</sub> with no evidence of impurity phases. The commercially available HfS<sub>2</sub> purchased for the program invariably contained small quantities of unidentifiable impurity phases.

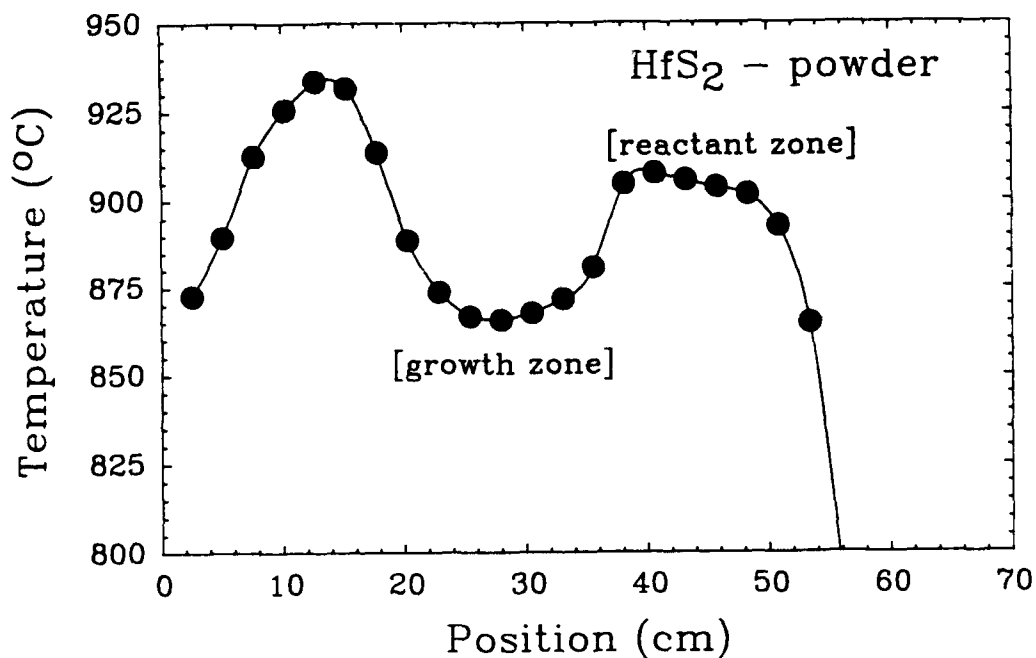


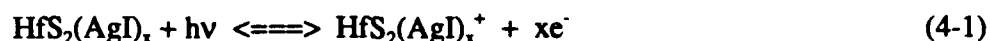
Figure 6. Temperature profile for preparation of HfS<sub>2</sub> "crystal-powder."

## SECTION 4

### INTERCALATION OF CHARGE TRANSFER COMPLEXES

#### 4.1 AgI IN HfS<sub>2</sub>.

The silver halides, particularly AgBr and AgI, are well known photoactive materials. Photon absorption in silver halide crystals produces a photoelectron and a positive hole. The objective of intercalating HfS<sub>2</sub> crystals with AgI is to use these photoelectrons to produce a semiconductor-to-metal transition under illumination. The photo-generated electrons should enter the conduction band of the HfS<sub>2</sub> crystal, leaving a positively charged ion in the van der Waals' gap. The overall reaction can be written



where the photoelectrons,  $xe^-$ , are in the HfS<sub>2</sub> conduction band. Silver, like the related alkali metals, can be readily intercalated into group IV dichalcogenides, although the intercalation reaction is less facile than with Li or Na.

Intercalation of the AgI charge transfer couple into the van der Waals' gaps of HfS<sub>2</sub> single crystal powder was attempted in two steps. In the first step, silver (Ag) was introduced into the gap by heating a mixture of finely divided Ag powder with HfS<sub>2</sub> crystal powder at 750°C for 4 days inside an evacuated quartz tube. The Ag intercalated HfS<sub>2</sub> powder was then heat treated at 400°C under 3 atmosphere of I<sub>2</sub> for 3 days inside an evacuated quartz tube.

Three different stoichiometric quantities of Ag intercalated HfS<sub>2</sub> were prepared according to the above procedure. Table 2 shows x-ray diffraction data for powders of nominal composition Ag<sub>0.1</sub>HfS<sub>2</sub>, Ag<sub>0.3</sub>HfS<sub>2</sub>, and Ag<sub>0.5</sub>HfS<sub>2</sub> following the 750°C diffusion heat treatment. Since the crystal powder is comprised of thin single crystal platelets which are crystallographically oriented with basal plane parallel with the faces of the platelets, packing the powder into the x-ray sample holder introduces a preferred orientation with the c-axes of the crystallites predominantly perpendicular to the sample surface. For this reason, the x-ray data on the crystal powder is comprised primarily of strong (00l) reflections with other reflections having low relative intensities ( $I/I_0 < 5\%$ ). There was no evidence of Ag peaks in the x-ray spectra as would be expected if all the Ag powder is consumed in the intercalation reaction. Energy dispersive x-ray analysis of the powder provided a qualitative indication of the presence of Ag.

The absence of a significant change in the lattice parameters of the Ag<sub>x</sub>HfS<sub>2</sub> powders is not necessarily surprising since the intercalated Ag<sup>+</sup> ions may counter the coulombic repulsion of the chalcogen layers. Positively charged Li<sup>+</sup> ions are known to cause a small contraction of the a axis in Li<sub>x</sub>ZrS<sub>2</sub> and Li<sub>x</sub>HfS<sub>2</sub> intercalation compounds and similar effects with the K<sup>+</sup>, Rb<sup>+</sup>, and Cs<sup>+</sup> intercalates of ZrS<sub>2</sub> have been observed (3). The Ag<sup>+</sup> ions probably reside on tetrahedral sites in the van der Waals' gaps. Since there are two distinct tetrahedral sites that have a temperature dependent occupancy, order-disorder transitions may be observed. Copper, which is similar to Ag as an intercalant, occupies tetrahedral sites in Ta and Nb chalcogenides and exhibits order-disorder transitions in both Cu<sub>x</sub>NbS<sub>2</sub> and Cu<sub>x</sub>TaS<sub>2</sub> that have been extensively characterized (3).

Table 2. X-ray data for  $\text{HfS}_2$  crystal powder and Ag intercalated powder.

$\text{HfS}_2$		$\text{HfS}_2(\text{Ag})_{0.1}$		$\text{HfS}_2(\text{Ag})_{0.3}$		$\text{HfS}_2(\text{Ag})_{0.5}$	
d(A)	hkl	d(A)	hkl	d(A)	hkl	d(A)	hkl
5.87	001	5.87	001	5.87	001	5.87	001
		3.14	100	3.14	100	3.14	100
2.93	002	2.93	002	2.93	002	2.93	002
2.78	101	2.77	101	2.76	101	2.77	101
2.15	102	2.14	102	2.14	102	2.14	102
1.95	003	1.95	003	1.95	003	1.95	003
		1.82	110	1.81	110	1.81	110
		1.73	111	1.73	111		
1.66	103	1.66	103	1.66	103	1.66	103
				1.51	201	1.52	201
1.47	004	1.47	004	1.47	004	1.47	004
		1.386	202			1.382	202
1.33	104	1.33	104			1.33	104

Following Ag intercalation, the  $\text{Ag}_x\text{HfS}_2$  powders were heat treated in an  $\text{I}_2$  atmosphere and analyzed by energy dispersive x-ray analysis (EDS). The EDS spectra of the  $\text{HfS}_2$ , clearly indicate the presence of both Ag and  $\text{I}_2$  in the treated powder (Figures 7-9). Prior to analysis, the  $\text{I}_2$  treated  $\text{Ag}_x\text{HfS}_2$  was thoroughly washed with anhydrous methanol to remove of any  $\text{I}_2$  or AgI that might reside on the surface of the powder.

To further investigate the nature of the iodine-treated  $\text{Ag}_x\text{HfS}_2$ , differential scanning calorimetry (DSC) was used in an effort to identify phase transformations that might be associated with intercalated iodine or a AgI complex. Figure 10 shows the DSC spectra of the three samples of  $(\text{AgI})_x\text{HfS}_2$  compared to a reference sample of AgI. For comparison, a spectrum of as-grown  $\text{HfS}_2$  crystal powder is shown in Figure 11. Silver iodide (AgI) has a melting point of  $558^\circ\text{C}$  and at  $146^\circ\text{C}$  there is an order-disorder phase transformation of hexagonal  $\alpha$ -AgI to cubic  $\beta$ -AgI. The DSC spectra of the  $\text{HfS}_2(\text{AgI})_x$  revealed endothermic reactions at the same phase transition temperature and melting point as the sample of pure AgI. The magnitude of the transitions increased with increasing Ag content as would be expected if the  $\text{I}_2$  treatment involves a reaction between iodine and intercalated Ag. X-ray diffraction analysis of the  $\text{I}_2$  treated  $\text{Ag}_x\text{HfS}_2$  powder, reported in Table II, revealed very weak ( $I/I_0 < 2\%$ ) (100), (002), and (110) reflections of  $\alpha$ -AgI. Residual AgI is, therefore, present in small amounts even though the powder was washed with methanol prior to x-ray and DSC analysis. These data demonstrate that Ag and  $\text{I}_2$  are reacting to form AgI.

A quantitative measure of the concentration of AgI intercalant or surface film on  $\text{HfS}_2$  was obtained from thermogravimetric analysis (TGA). Weight loss versus temperature plots of  $\text{HfS}_2$  crystal powder, Ag intercalated  $\text{HfS}_2$ , various  $\text{I}_2$  treated  $\text{Ag}_x\text{HfS}_2$  powders, and pure AgI are compared in Figure 12. Figure 13 compares the TGA spectra of  $\text{Ag}_x\text{HfS}_2(\text{I}_2)$  for  $x = 0.1, 0.3$ , and  $0.5$  with pure AgI. The weight loss increases with increasing Ag content of the powder, implying that the  $\text{I}_2$  has reacted with the intercalated Ag to form AgI. There is no corresponding weight loss for  $\text{Ag}_x\text{HfS}_2$  crystal powder that has not been treated with iodine. Assuming that the weight loss between  $600^\circ\text{C}$  and  $1000^\circ\text{C}$  is due to AgI (melting point  $558^\circ\text{C}$ ), Table 3 shows the calculated AgI stoichiometries for different  $\text{Ag}_x\text{HfS}_2$  compositions. As expected, the AgI stoichiometry increases

with increasing Ag content. The AgI mole fractions are lower than the Ag mole fractions in the formulated  $\text{Ag}_x\text{HfS}_2$  powder. This is probably due to less than nominal stoichiometric incorporation of Ag during the Ag/HfS<sub>2</sub> intercalation diffusion heat treatments or incomplete reaction of I<sub>2</sub> with the intercalated Ag.

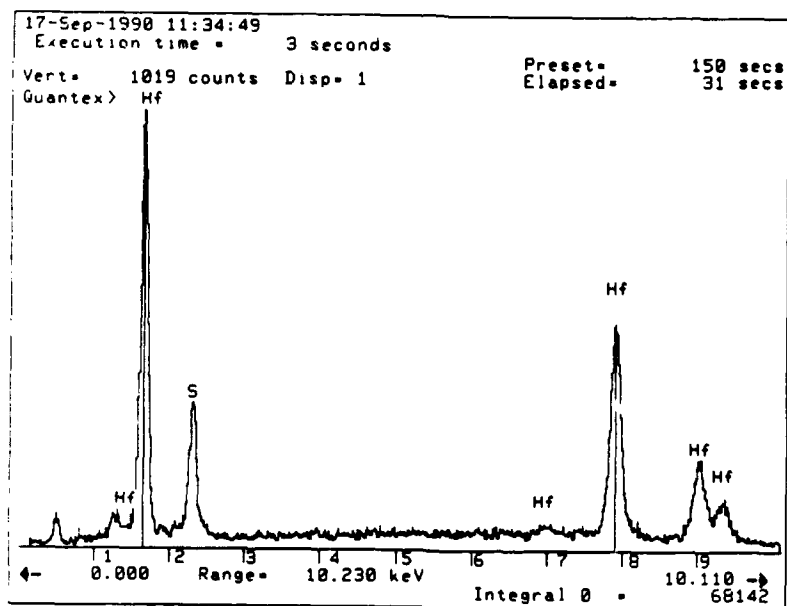


Figure 7. EDS spectrum of as-grown HfS<sub>2</sub> crystal-powder.

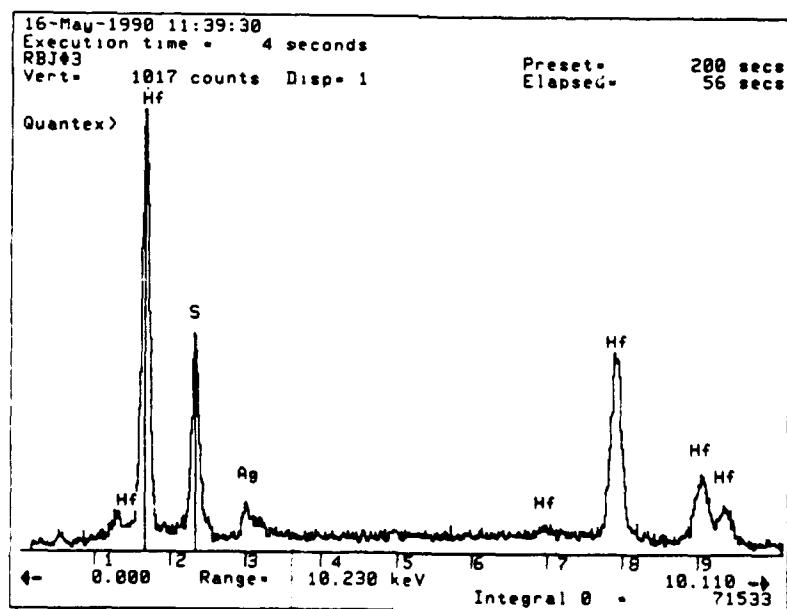


Figure 8. EDS spectrum of HfS<sub>2</sub> crystal powder showing the presence of Ag in the HfS<sub>2</sub> following a 750°C diffusion anneal with Ag powder.

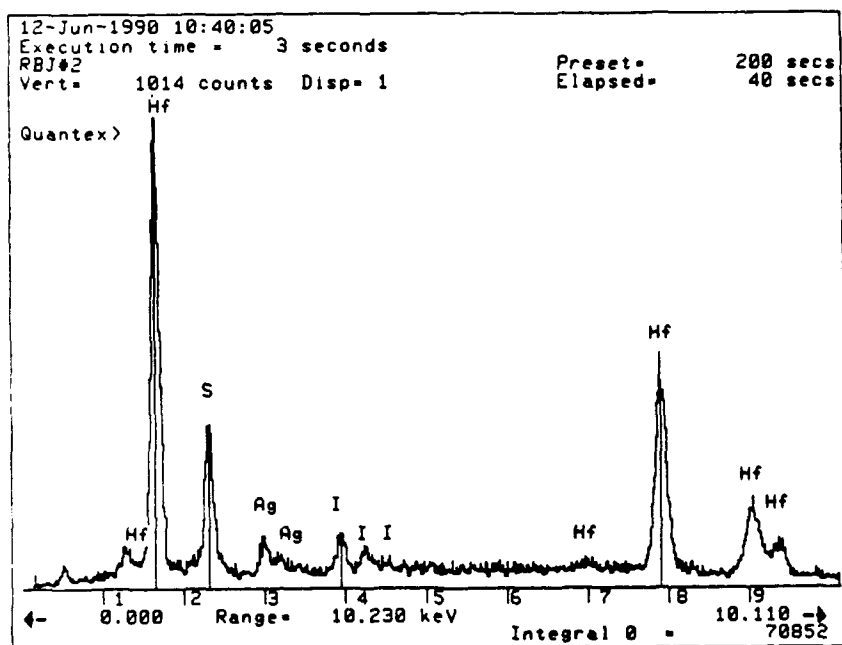


Figure 9. EDS spectrum of  $\text{Ag}_x\text{HfS}_2$  powder following a  $400^\circ\text{C}$  treatment in  $\text{I}_2$ . Both Ag and I are present in the spectrum.

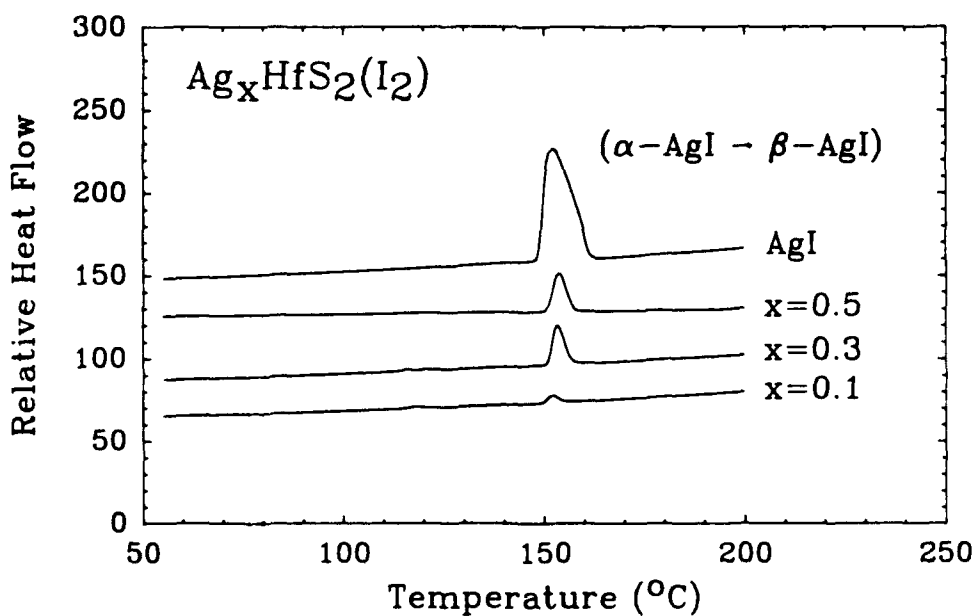


Figure 10. DSC spectra of  $\text{Ag}_x\text{HfS}_2$  crystal powder following treatment in  $\text{I}_2$ .

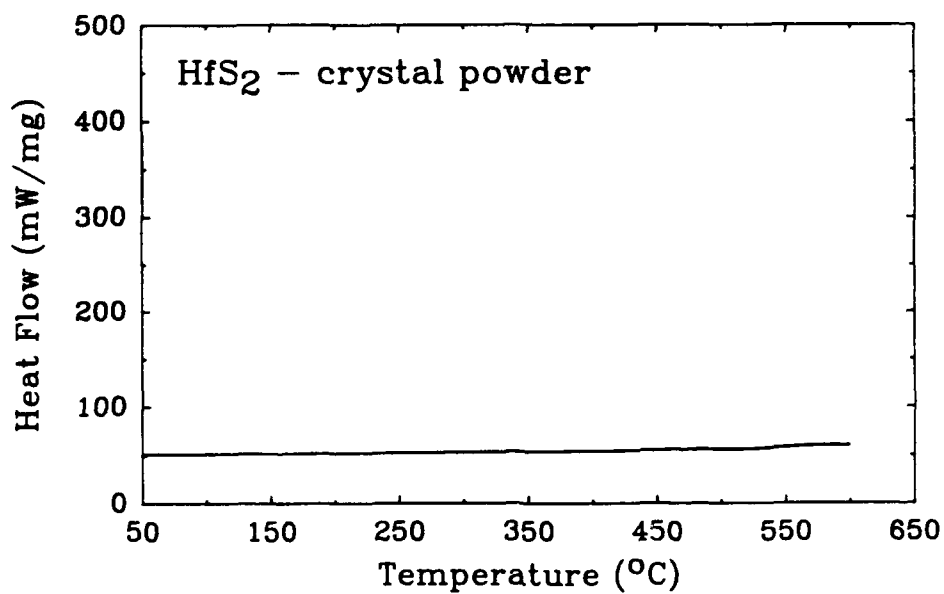


Figure 11. DSC spectrum of as-grown  $\text{HfS}_2$  crystal powder.

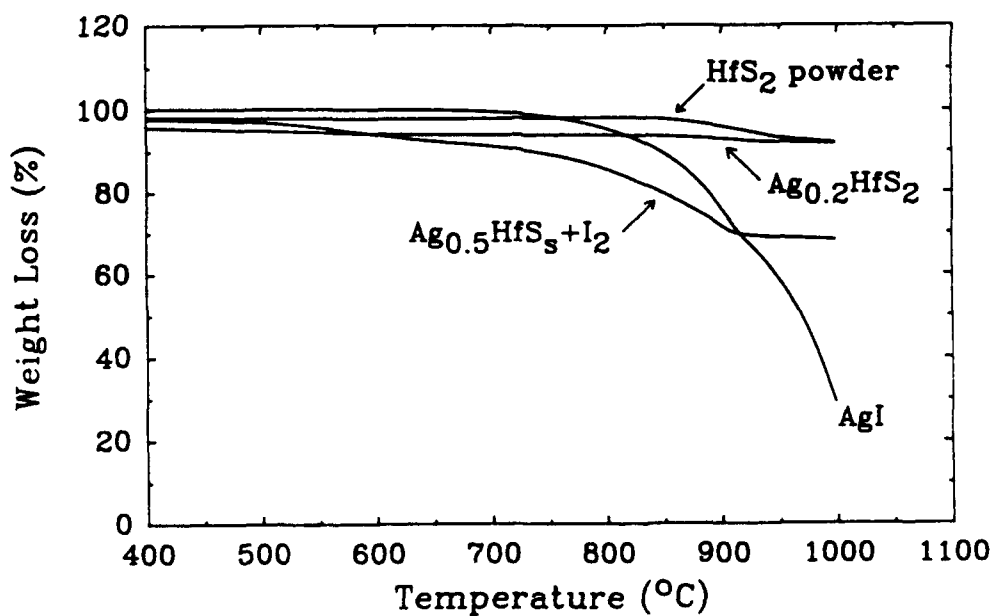


Figure 12. Thermogravimetric analysis of  $\text{HfS}_2$ ,  $\text{Ag}_x\text{HfS}_2$ , and  $\text{Ag}_x\text{HfS}_2$  ( $\text{I}_2$  treated).

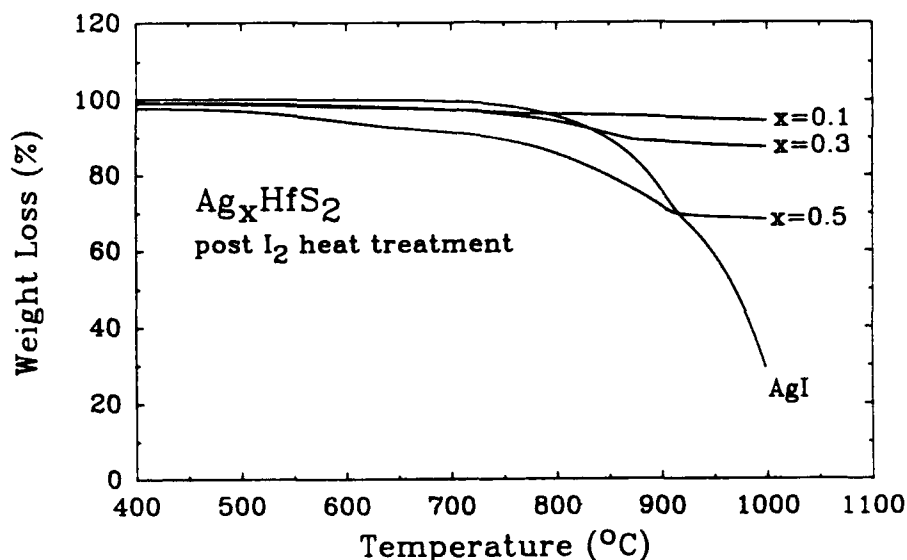


Figure 13. Thermogravimetric analysis of AgI and  $\text{Ag}_x\text{HfS}_2(\text{I}_2)$  for  $x = 0.1$ ,  $0.3$ , and  $0.5$ .

Table 3. AgI stoichiometry from TGA results.

Nominal Ag Stoichiometry $x$ in $\text{Ag}_x\text{HfS}_2$	Weight Loss (%)	Calculated AgI Stoichiometry $x$ in $(\text{AgI})_x\text{HfS}_2$
0.1	5.6	0.06
0.3	12.7	0.14
0.5	22.3	0.29

The results from X-ray, EDS, DSC, and TGA analysis of  $\text{HfS}_2$  powder following Ag intercalation and attempts to intercalate iodine are inconclusive as to the nature of the intercalated species. In particular, the data are unable to differentiate between iodine that has intercalated into the  $\text{Ag}_x\text{HfS}_2$  to form  $(\text{AgI})_x\text{HfS}_2$  or has extracted Ag from  $\text{Ag}_x\text{HfS}_2$  to form an AgI surface film. Infrared spectroscopy and Auger analysis of  $\text{HfS}_2$  single crystals following Ag intercalation and  $\text{I}_2$  treatment were undertaken in an effort to conclusively identify the reaction between  $\text{Ag}_x\text{HfS}_2$  and iodine.

#### 4.2 INTERCALATION OF Ag AND $\text{I}_2$ INTO $\text{HfS}_2$ SINGLE CRYSTALS.

The infrared (2-16  $\mu\text{m}$ ) optical properties of a  $\text{HfS}_2$  single crystal after Ag intercalation and reaction with  $\text{I}_2$  were studied by transmittance in a Fourier transform infrared spectrophotometer. Silver was intercalated into the single crystal by thermally evaporating a thin film of Ag onto the crystal and diffusing the Ag into the bulk by a diffusion heat treatment at  $625^\circ\text{C}$  for 72 hr. The  $\text{HfS}_2$  crystals were maintained at a substrate temperature of  $300^\circ\text{C}$  during Ag evaporation, which was insufficient to cause significant intercalation. The Ag stoichiometry was calculated from the increase in weight following deposition. Following an initial diffusion heat-treatment at  $500^\circ\text{C}$ , the coated crystals retained a metallic silvery appearance and a strong Ag reflection was evident in

the x-ray diffraction spectra. After increasing the diffusion temperature to 625°C, the crystals became reddish-purple in color and the Ag peak disappeared from the x-ray spectra. Silver was intercalated by this method to a maximum average concentration of  $\text{Ag}_{0.05}\text{HfS}_2$ . X-ray diffraction spectra of the Ag intercalated crystal did reveal a slight expansion of the c-axis at a composition of  $\text{Ag}_{0.05}\text{HfS}_2$ . Following Ag intercalation, the crystal was heat-treated at 400°C under 4 atmospheres of  $\text{I}_2$  in an evacuated and sealed quartz tube.

The FTIR transmittance spectra, normal to the basal plane, of the  $\text{HfS}_2$  single crystal at various steps of intercalation are shown in Figure 14. The as-grown crystal is about 65% transmissive across the 2.5-16  $\mu\text{m}$  wavelength region. The maximum transmission at normal incidence through a thin sheet of material in air is,

$$T = (1 - R')^2 = \left( 1 - \left( \frac{n - 1}{n + 1} \right)^2 \right)^2 \quad (4 - 2)$$

where  $R'$  is the reflectance of a single air-crystal interface and  $n$  is the refractive index of the crystal. The index of refraction of  $\text{HfS}_2$  is estimated from Bell and Liang (4) to be 2.87 at 10  $\mu\text{m}$ , which yields a transmittance of 59% for  $\text{HfS}_2$  in agreement with the experimental results. The transmittance of the thin  $\text{HfS}_2$  crystals is limited by the mismatch in refractive indices. With an appropriate antireflection coating, higher transmittance values would be obtained.

With the intercalation of Ag, the transmittance of the crystal rapidly decreases. The reduction in transmittance is due to the large increase in reflectance associated with a high free-electron density following Ag intercalation. The higher transmittance at the shorter wavelengths probably signifies the onset of the Drude edge. After treatment in  $\text{I}_2$  (4 atm at 400°C) for 72 hours the crystal regained a substantial proportion of its as-grown transmittance, exhibiting a broadband transmittance of 40%. The increase in transmittance is due to reaction of the Ag with the  $\text{I}_2$  to form AgI, with a corresponding loss of conduction electrons as the Ag  $5s^1$  electron becomes localized on the I anion. EDS analysis of the crystal indicated the presence of iodine although no Ag peaks were evident in the spectrum.

Changes in the electrical resistivity parallel to the c-axis of the crystal were measured after Ag intercalation and  $\text{I}_2$  treatment. The resistivities were determined using the van der Pauw technique and are summarized in Table 4 (5,6). The van der Pauw technique can be used to measure the electronic resistivity of an arbitrarily shaped flat sample and is well suited to the characterization of dichalcogenide crystals. The as-grown crystal had a resistivity of  $2.3 \times 10^4 \Omega\text{-cm}$  at 25°C which decreased to 19.4  $\Omega\text{-cm}$  after Ag intercalation to  $\text{Ag}_{0.05}\text{HfS}_2$ . This comparatively low resistivity is expected since the average free-electron density, assuming 100% ionization of the Ag, is  $\sim 8 \times 10^{20} \text{ e}^-/\text{cm}^3$ . Following the  $\text{I}_2$  treatment, the resistivity increased to a value higher than that measured in the as-grown crystal. The behavior of the resistivity at 77 K (in liquid nitrogen) differed markedly. After Ag intercalation the resistivity increased by one order of magnitude and further increased after  $\text{I}_2$  treatment. The low electrical conductivity of  $\text{Ag}_{0.05}\text{HfS}_2$  at 77 K suggests that the intercalated Ag is not ionized at this temperature.

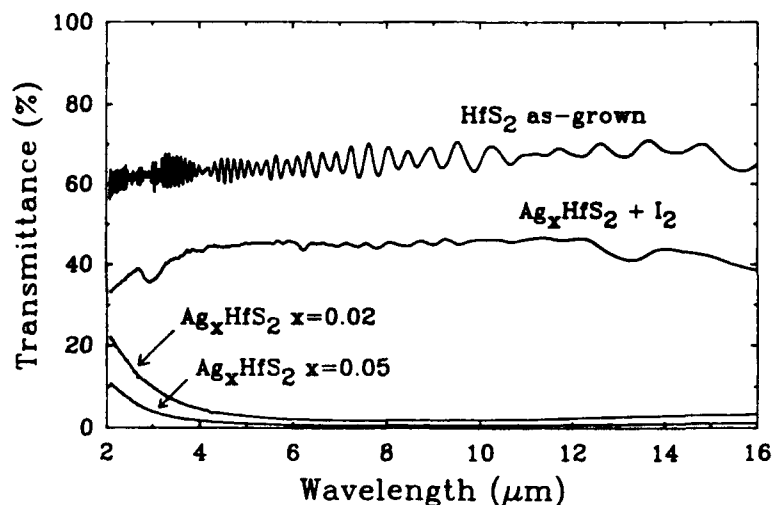
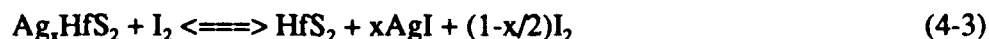


Figure 14. Infrared transmittance of a  $\text{HfS}_2$  single crystal following successive Ag intercalation and treatment with  $\text{I}_2$ . The incident beam is perpendicular to the basal plane.

Table 4. van der Pauw electrical resistivity parallel to the c-axis of  $\text{Ag}_x\text{HfS}_2$ .

Temperature	Resistivity (ohm-cm)		
	$\text{HfS}_2$ Crystal	$\text{HfS}_2(\text{Ag})_{0.05}$	$\text{HfS}_2(\text{AgI})_{0.05}$
25°C	$2.3 \times 10^4$	19.4	$5.3 \times 10^4$
-196°C	$9.1 \times 10^5$	$9.1 \times 10^6$	$6.4 \times 10^7$

The electrical resistivity and optical changes following Ag intercalation and treatment in  $\text{I}_2$  are consistent with formation of AgI. X-ray diffraction, DSC, and TGA data confirm the presence of AgI, but it is not clear whether the  $\text{I}_2$  "extracts" Ag from  $\text{Ag}_x\text{HfS}_2$  to form a surface layer of AgI or whether  $\text{I}_2$  has intercalated to form a AgI complex in the van der Waals' gap. To resolve this issue, compositional depth profiling using scanning Auger spectroscopy of an  $\text{I}_2$  treated  $\text{Ag}_{0.05}\text{HfS}_2$  crystal was employed. The crystal was thoroughly washed with methanol prior to Auger analysis and then sputtered *in situ* with argon for 45 minutes until the oxygen signal was reduced to background levels. Extensive sputter cleaning of the surface is necessary to remove corrosion products associated with the reaction of  $\text{HfS}_2$  with water vapor. The Auger spectra contained no evidence of Ag or I, even though both sides of the crystal were profiled. The absence of Ag or I in the crystal suggests that  $\text{I}_2$  deintercalates Ag from the crystal with the concomitant formation of AgI on the crystal surface. The overall reaction being



The extraction of Ag from the  $\text{HfS}_2$  indicates that electron donor intercalation followed by reaction with an electron acceptor will not form a charge transfer complex in the van der Waals gap of  $\text{HfS}_2$ . The situation is probably the same for other dichalcogenide crystals as well.

## SECTION 5

### MIXED-METAL DICHALCOGENIDES

The purpose of intercalating a charge transfer complex is to provide an electro- or photoactive center in the van der Waals' gap of the dichalcogenide crystal. Activation of the complex (e.g. AgI) should result in the valence electron from the Ag entering the conduction band of the crystal causing, when a sufficient density of electrons is achieved, a semiconductor to metal transition. Since efforts at complex formation by reaction of intercalated Ag with  $I_2$  were unsuccessful, a second approach was taken. In this case, the crystal was doped with an electron donor by substituting a group V metal (V, Nb, or Ta) for part of the Hf during the crystal growth process. Since the group V metal acts as a substitutional n-type donor, the crystal should exhibit metallic behavior and infrared reflectivity. The magnitude of the reflectance depends on the dopant concentration ( $x$ ) which determines the density of itinerant electrons in the conduction band and also the electrical conductivity of the crystal which is determined by the electron density and scattering. The primary source of electron scattering is probably the group V metal atoms which act as ionized impurities. Based on unit cell parameters of  $a=3.623\text{\AA}$  and  $c=5.841\text{\AA}$ , a substitution of  $x=0.1$  would result in a free-electron density of  $1.5 \times 10^{21} \text{ e}^-/\text{cm}^3$ , assuming all the donors are ionized.

#### 5.1 GROWTH AND CHARACTERIZATION OF MIXED-METAL CRYSTALS.

Closed-tube-vapor-transport (CTVT) of  $\text{Hf}_{1-x}\text{M}_x\text{S}_2$  ( $\text{M}=\text{V}$ , Nb, and Ta) single crystals was accomplished using the typical time-temperature profiles described previously, except that lower temperature gradients across the growth zone ( $2^\circ\text{C}/\text{cm}$  versus  $4^\circ\text{C}/\text{cm}$  for  $\text{HfS}_2$ ) and longer growth times were required to obtain large crystals. The as-grown crystals were characterized optically by IR transmittance and hemispherical reflectance measurements and electrical by van der Pauw measurements. In order to compensate the excess free-electrons in the as-grown crystals, efforts were made to intercalate the electron acceptors  $I_2$  and  $\text{Br}_2$ . Successful intercalation of these materials should result in an increase in resistivity and an increase in IR transmittance, both due to localization of free-electrons.

The results of the van der Pauw measurements of electrical resistivity are listed in Table 5 for a variety of mixed-metal crystals and a  $\text{HfS}_2$  control crystal. A resistivity of  $1 \times 10^7 \Omega\text{-cm}$  for the as-grown  $\text{HfS}_2$  crystal agrees fairly well with data previously reported (7). As-expected, the electrical resistivities of the mixed-metal crystals were lower than the  $\text{HfS}_2$ . The lowest resistivity recorded was  $4 \times 10^5 \Omega\text{-cm}$  for  $\text{Hf}_{0.9}\text{Nb}_{0.1}\text{S}_2$  which is a 25-fold increase in conductivity over  $\text{HfS}_2$ . The reduced resistivity arises from the n-type doping introduced by the group V metal substituent.

The IR optical properties of the crystals were examined in transmission with an FTIR. The crystals exhibited a featureless, broadband transmittance between 20% and 50% over the 2-16  $\mu\text{m}$  wavelength region. There was no correlation between transmittance and the concentration of group V dopant. In addition, even for the crystals containing 0.3 mole fraction of the group V metal, the transmittance was not decreased below 20%. Obviously, the doped crystals are not developing the high degree of reflectance required for optical hardening. This result is not unexpected in light of the modest gains in electrical conductivity obtained by substitutional doping (see Table 5). Significantly higher conductivities would be required if the doped crystals were to exhibit the high

reflectivities associated with the metallic behavior of the silver intercalated crystals. It is unlikely that the mixed-metal crystals will have sufficient reflectivity for optical hardening without an additional source of electrons.

Table 5. Compilation of data on mixed-metal dichalcogenide crystals as-grown and after treatment in  $I_2$  vapor.

Crystal	Resistivity ( $\Omega$ -cm)	Thickness (mm)	Diameter of Largest Crystal (mm)
HfS <sub>2</sub> as-grown	$1 \times 10^7$	0.051	17
$I_2$ treated	$3 \times 10^6$		
Hf <sub>0.9</sub> V <sub>0.1</sub> S <sub>2</sub> as-grown	$3 \times 10^6$	0.140	10
$I_2$ treated	$1 \times 10^7$		
Hf <sub>0.9</sub> Nb <sub>0.1</sub> S <sub>2</sub> as-grown	$4 \times 10^5$	0.106	9
$I_2$ treated	$9 \times 10^6$		
Hf <sub>0.9</sub> Ta <sub>0.1</sub> S <sub>2</sub> as-grown	$2 \times 10^6$	0.071	4
Hf <sub>0.7</sub> V <sub>0.3</sub> S <sub>2</sub> as-grown	$6 \times 10^6$	0.094	6
$I_2$ treated	$2 \times 10^7$		
Hf <sub>0.7</sub> Nb <sub>0.3</sub> S <sub>2</sub> as-grown	$2 \times 10^6$	0.168	12

## 5.2 HALIDE INTERCALATION.

The original idea behind the use of mixed-metal crystals was to create an energetically favorable environment for electron-acceptor intercalation into the dichalcogenides. Both iodine and bromine intercalation were investigated.

Iodine intercalation was attempted by heating crystals in 6 atmospheres of  $I_2$  vapor at 300-400°C for times varying from 2-250 hours. The crystals were characterized by x-ray diffraction, EDS, and van der Pauw measurements of electronic resistivity. X-ray diffraction results are given in Tables 6-10 for a HfS<sub>2</sub> control crystal, Hf<sub>0.9</sub>V<sub>0.1</sub>S<sub>2</sub>, Hf<sub>0.9</sub>Nb<sub>0.1</sub>S<sub>2</sub>, Hf<sub>0.9</sub>Ta<sub>0.1</sub>S<sub>2</sub>, and Hf<sub>0.7</sub>V<sub>0.3</sub>S<sub>2</sub>. The x-ray diffraction data indicate that the mixed-metal crystals maintain the hexagonal structure of the host HfS<sub>2</sub> without significant changes in the c lattice parameter. The only reflections evident in the diffraction patterns are of the type (00l) corresponding to the different orders of the basal plane. There is no change in the diffraction data of the crystals after heat treatment in  $I_2$ , indicating very little if any intercalation. The absence of  $I_2$  intercalation was further suggested by qualitative EDS analysis. Occasionally, small quantities of  $I_2$  were identified in the EDS spectra. This  $I_2$ , however, could also be attributed to residual surface contamination following the heat treatment even though the crystals were washed with methanol and carbon tetrachloride.

The electronic conductivities of the mixed-metal crystals showed a significant decrease after treatment in  $I_2$ , as would be expected for compensation of electron donors. However, scanning electron microscopy indicated varying degrees of exfoliation of the crystals which would also decrease conductivity. The  $Hf_{0.9}Ta_{0.1}S_2$  crystal, for example, was sufficiently exfoliated that it was not possible to perform a post-heat treatment resistivity measurement. Figure 15 shows a scanning electron micrograph of a  $Hf_{0.9}Nb_{0.1}S_2$  crystal partially exfoliated. Heat treating the crystals at  $300^\circ C$  without  $I_2$  produced no evidence of exfoliation.

In total, these results suggest that  $I_2$  is not intercalating into the mixed-metal dichalcogenide crystals, at least in the conventional sense in which the characteristics of the host and guest species are preserved. Rather, the  $I_2$  is entering the van der Waals' gaps of the crystals and causing physical debonding of the layers with resulting macroscopic exfoliation. The origin of the debonding is probably coulombic repulsion between the  $I_2$  and the electronegative chalcogen (sulfur) layers adjacent to the gap. Silver on the other hand, after donating its 5s electron to the host crystal, is positively charged and stabilizes the crystal through coulombic interactions.

Bromine intercalation by exposure of mixed-metal crystals to liquid bromine or bromine/ethanol solutions also produced exfoliation of the crystals and in some cases produced a needle-like phase indicating decomposition of the dichalcogenide. We conclude, therefore, that direct intercalation of  $I_2$  and  $Br_2$  as electron acceptors in  $HfS_2$  and mixed-metal crystals is unlikely to be successful.

Table 6.  $HfS_2$  before and after  $I_2$  intercalation experiments.

Before Intercalation		After Intercalation		
d (Å)	I/I <sub>0</sub>	d (Å)	I/I <sub>0</sub>	hkl
5.85	100	5.85	100	001
2.931	20	2.928	27	002
1.952	58	1.951	33	003
1.4636	62	1.4631	28	004
1.1705	15	1.1703	5	005

Table 7.  $Hf_{0.9}V_{0.1}S_2$  before and after  $I_2$  intercalation experiments.

Before Intercalation		After Intercalation		
d (Å)	I/I <sub>0</sub>	d (Å)	I/I <sub>0</sub>	hkl
5.83	100	5.81	100	001
2.922	24	2.919	27	002
1.947	43	1.948	24	003
1.4623	50	1.4615	21	004
1.1702	20	1.1694	4	005

Table 8.  $\text{Hf}_{0.9}\text{Nb}_{0.1}\text{S}_2$  before and after  $\text{I}_2$  intercalation experiments.

Before Intercalation		After Intercalation		
d (Å)	I/I <sub>0</sub>	d (Å)	I/I <sub>0</sub>	hkl
5.86	100	5.86	100	001
2.931	36	2.929	57	002
1.952	36	1.952	65	003
1.4636	35	1.4627	54	004
1.1705	10	1.1701	22	005

Table 9.  $\text{Hf}_{0.9}\text{Ta}_{0.1}\text{S}_2$  before and after  $\text{I}_2$  intercalation experiments.

Before Intercalation		After Intercalation		
d (Å)	I/I <sub>0</sub>	d (Å)	I/I <sub>0</sub>	hkl
5.85	100	5.84	100	001
2.928	26	2.925	26	002
1.952	32	1.952	31	003
1.4627	22	1.4624	24	004
1.1702	6	1.1702	7	005

Table 10.  $\text{Hf}_{0.7}\text{V}_{0.3}\text{S}_2$  before and after  $\text{I}_2$  intercalation experiments.

Before Intercalation		After Intercalation		
d (Å)	I/I <sub>0</sub>	d (Å)	I/I <sub>0</sub>	hkl
5.84	100	5.84	100	001
2.922	27	2.923	43	002
1.950	35	1.950	57	003
1.4623	31	1.4620	59	004
1.1702	8	1.1701	20	005

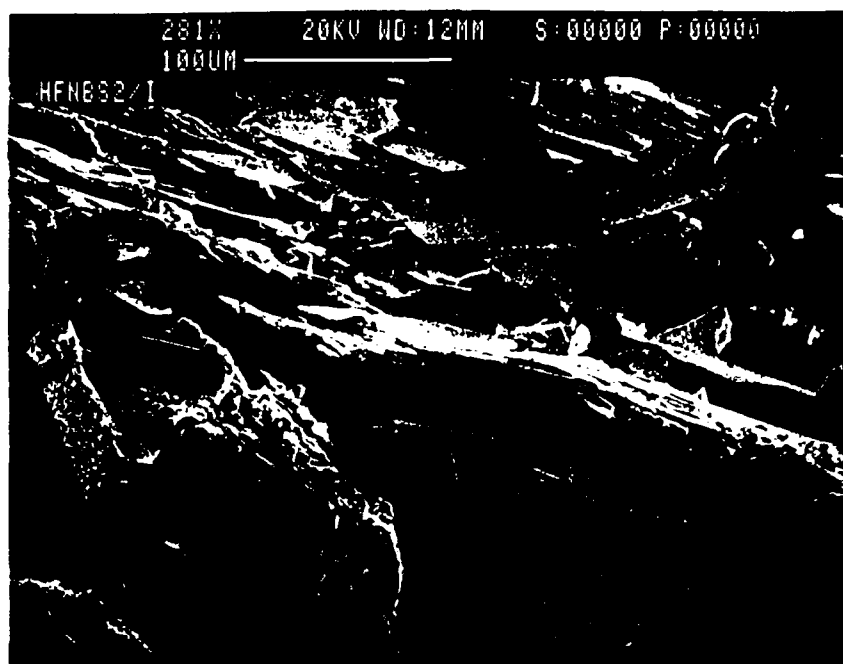


Figure 15. Scanning electron micrograph of a partially exfoliated  $\text{Hf}_{0.9}\text{Nb}_{0.1}\text{S}_2$  crystal after heat treatment in  $\text{I}_2$  at  $300^\circ\text{C}$ .

## SECTION 6

### METALLOCENE INTERCALATION

The observation that  $I_2$  cannot be intercalated into group IV or mixed IV-V dichalcogenides without extracting the intercalated electron donor as in the case of  $Ag_xHfS_2$  or exfoliation as in the case of the mixed-metal crystals, necessitated a different approach to forming intercalated charge-transfer complexes. To preserve the structure of the dichalcogenide host and allow intercalation of guest species which are not energetically favored, intercalation of relatively large electron donor molecules which significantly expand the van der Waals gap was investigated. In this approach, the metallocenes, ferrocene  $(C_2H_5)_2Fe$ , cobaltocene  $(C_2H_5)_2Co$  and chromocene  $(C_2H_5)_2Cr$ , were intercalated into  $HfS_2$  and  $ZrS_2$  crystal-powder to expand the c-axis and act as electron donors.

Metallocenes are metallorganic molecules containing a central, multivalent metal ion sandwiched between two cyclopentadienyl rings. Metallocenes such as cobaltocene or chromocene will spontaneously intercalate into the van der Waals' gap of the group IVB and group VB dichalcogenides leading to the expansion of the c-axis by about 5.5 Å (8). The increase in the c-axis lattice should facilitate the introduction of  $I_2$  which readily forms charge transfer adducts with metal chelates containing an aromatic ring (9).

To determine the feasibility of this approach, commercially available dichalcogenide powders were used as a host structure rather than single crystals. Powders reduce the time necessary for diffusion of the intercalants into the van der Waals' gap of the dichalcogenides and expedite sample preparation.

The intercalation of ferrocene into metal dichalcogenides was attempted by soaking the host  $HfS_2$  and  $ZrS_2$  chalcogenides in a 0.5M solution of ferrocene (Aldrich Chemicals) in cyclooctane. The mixture was heated to 105°C under constant stirring for 6 and 12 days for the  $HfS_2$  and  $ZrS_2$ , respectively. The intercalation was performed in a Vacuum Atmospheres' dry box, catalytically purged of  $H_2O$ . After the intercalation treatment, the metal dichalcogenide powders were filtered and thoroughly washed with hexane and dried under vacuum.

To determine the degree of intercalation of ferrocene into the van der Waals' gap of the powder, three analytical techniques were utilized: x-ray diffraction, Fourier Transform IR spectroscopy, and compositional analysis by energy dispersive x-ray spectroscopy.

Table 11 shows the x-ray diffraction spectra of  $HfS_2$  before and after intercalation. The x-ray data reveal that the as-received  $HfS_2$  (Strem Chemicals) has an expanded c-axis, indicating a significant deviation from ideal stoichiometry. After treatment in the ferrocene/cyclooctane solution, the lattice parameter decreased to a value closer to that obtained with a single crystal or crystal-powder. However, there was no evidence of a low angle reflection that might indicate a significant c-axis expansion that would accompany ferrocene intercalation. The x-ray diffraction analysis of the  $ZrS_2$  after the intercalation reaction with ferrocene (Table 12) also shows no change in lattice parameter, indicating that no intercalation had occurred. Further qualitative compositional analysis with EDS confirmed the absence of iron, and the FTIR spectrum of the treated powder did not reveal absorption peaks associated with the cyclopentadienyl group. Dines (8) has reported

that the reactivity of the guest metallocene is critically dependent on its ionization potential. Presumably, the ionization potential of ferrocene is high enough to create an energetically unfavorable situation for the intercalation reaction to occur.

Table 11.  $\text{HfS}_2$  before and after ferrocene intercalation.

Before Intercalation		After Intercalation		
d(A)	I/I <sub>0</sub>	d(A)	I/I <sub>0</sub>	hkl
6.068	72	5.829	72	001
3.209	100	3.121	100	100
2.871	52	2.806	55	002
2.814	82	2.747	66	?
2.652	31	2.600	27	?
2.557	22	2.515	23	?
2.166	35			102
1.831	36	1.804	44	110
1.746	27			111

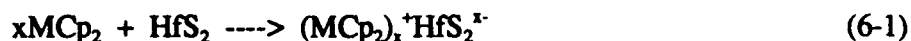
Table 12.  $\text{ZrS}_2$  before and after ferrocene intercalation.

Before Intercalation		After Intercalation		
d(A)	I/I <sub>0</sub>	d(A)	I/I <sub>0</sub>	hkl
5.915	88	5.907	100	001
3.195	35	3.187	31	100
2.801	100	2.800	95	101
2.156	52	2.156	42	102
1.837	41	1.838	27	110
1.752	27	1.753	15	111
1.661	21	1.658	10	103
1.59	12			200
1.535	20	1.533	9	112
1.47	12			004
1.396	18	1.393	7	202
1.336	13			113
1.231	13			203
1.202	11			210
1.176	15	1.176	7	211

On the other hand, the intercalation of cobaltocene and chromocene, two members of the metallocene group with lower ionization potentials, into  $\text{HfS}_2$  or  $\text{ZrS}_2$  should be energetically more favorable. The intercalation of cobaltocene into  $\text{HfS}_2$  was accomplished by heating a mixture of  $\text{HfS}_2$  single crystal powder (2 gm) in 25 cc of cobaltocene solution (0.22M) with cyclooctane as a solvent at 105-110°C under constant stirring for three days. The  $\text{HfS}_2$  single crystal powder was

then filtered out, washed thoroughly with hexane, and dried under vacuum. Chromocene was also intercalated into HfS<sub>2</sub> single crystal powder in the same manner, except that the reaction time was increased to seven days.

The cobaltocene intercalated crystal powder became dark black whereas the chromocene intercalated material became dark black with a dark green tone. This darkening of the crystal is probably the result of the ionization of the intercalated metallocenes promoting free electrons into the conduction band of the HfS<sub>2</sub> host lattice:



X-ray diffraction patterns of the HfS<sub>2</sub> single crystal powder (Table 13) before and after intercalation indicate that the d spacing of the (001) basal plane has expanded to 11.63Å, corresponding to a dilation of 5.8Å in the layer-to-layer spacing of the HfS<sub>2</sub> host structure for both cobaltocene and chromocene intercalation. This c-axis expansion is quite reasonable, since metallocenes have a dimension of approximately 6.8Å along their C5 axis and 5.65Å across this axis. The intercalated metallocene, therefore, seems to be located inside the van der Waals' gap with its cyclopentadienyl rings perpendicular to the layers of the host structure.

The presence of intercalated metallocene is further confirmed by EDS. The EDS spectra of HfS<sub>2</sub> after treatment with cobaltocene and chromocene are shown in Figures 16 and 17, respectively. Both Co and Cr are present in the HfS<sub>2</sub> after the metallocene intercalation reaction. The EDS spectrum of as-grown HfS<sub>2</sub> crystal powder is shown in Figure 18 for comparison. Occasionally, very small quantities of the iodine transport agent are observed in the spectra of as-grown crystals or powder.

Table 13. HfS<sub>2</sub> single crystal powder with metallocene intercalation.

Cobaltocene Intercalation			Chromocene Intercalation		
d(Å)	I/I <sub>0</sub>	hkl	d(Å)	I/I <sub>0</sub>	hkl
11.633	100	001	11.633	38	001
5.754	66	002	5.792	100	002
3.726	5	003	3.834	5	003
3.100	1		3.143	2	
2.858	5	004	2.867	6	004
2.550	1		2.293	3	005
2.282	3	005	2.151	3	
2.217	1		1.949	4	006
2.006	1		1.661	2	
1.903	3	006	1.637	3	007
1.631	2	007	1.463	2	
1.427	2	008	1.433	2	008

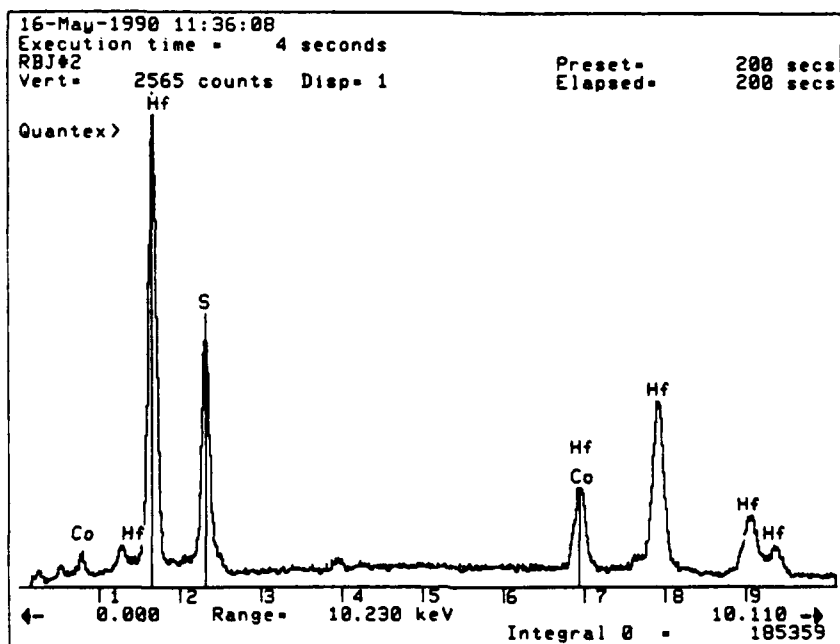


Figure 16. EDS spectrum of  $\text{HfS}_2$  following cobaltocene intercalation.

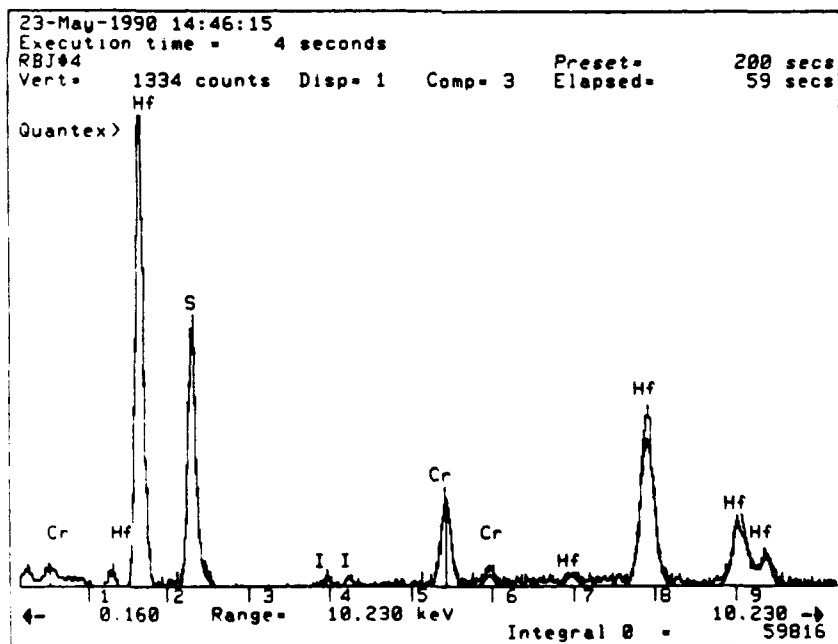


Figure 17. EDS spectrum of  $\text{HfS}_2$  following chromocene intercalation.

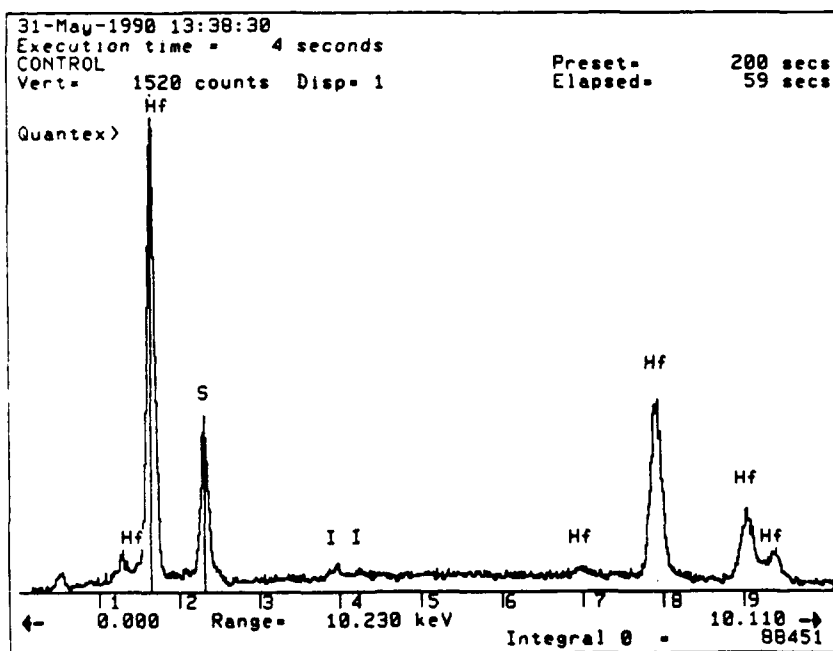


Figure 18. EDS spectrum of as-grown  $\text{HfS}_2$  crystal powder.

## 6.1 METALLOCENE - $\text{I}_2$ INTERCALATION.

Following the successful intercalation of cobaltocene and chromocene into the van der Waals' gap of  $\text{HfS}_2$  and  $\text{ZrS}_2$  powder, the formation of a charge transfer adduct with  $\text{I}_2$  as an electron acceptor was investigated.

The preparation of the charge transfer adduct was accomplished by heating a mixture of cobaltocene intercalated  $\text{HfS}_2$  single crystal powder with  $\text{I}_2$  inside an evacuated and sealed quartz tube which was heated to  $300^\circ\text{C}$  for three days. The excess  $\text{I}_2$  was removed by sublimation and the remaining powder washed with methanol to further remove residual traces of unreacted  $\text{I}_2$ .

X-ray diffraction patterns of the  $\text{I}_2$ -treated  $\text{HfS}_2$  single crystal powder (Table 14) showed the disappearance of the peak at a d-spacing of  $11.63\text{\AA}$  for both the chromocene and cobaltocene intercalated material. This seems to indicate that metallocenes have been deintercalated from the van der Waals' gap during the gas phase reaction with  $\text{I}_2$ .

On the other hand, results from qualitative EDS analysis (Figures 19 and 20) clearly confirm the presence of I (iodine) as well as Co and Cr in the  $\text{HfS}_2$  single crystal powder. Qualitatively, there is a greater concentration of Cr and I present in the chromocene intercalated sample than Co and I in the cobaltocene intercalated sample. The reason for this will become apparent from thermogravimetric analysis. The intensity of the iodine peaks in the EDS spectra are greater than that observed with  $\text{I}_2$  treated  $\text{Ag}_x\text{HfS}_2$  in which a small amount of  $\text{AgI}$  remained on the crystal surface after the  $\text{I}_2$  had extracted the Ag to form  $\text{AgI}$  which was subsequently removed by washing with methanol. Thus, the metallocenes and iodine appear to exist simultaneously in the  $\text{HfS}_2$  single crystal powder. It is not known whether the iodine has formed an adduct with the metallocenes or exists independently as  $\text{I}_2$ .

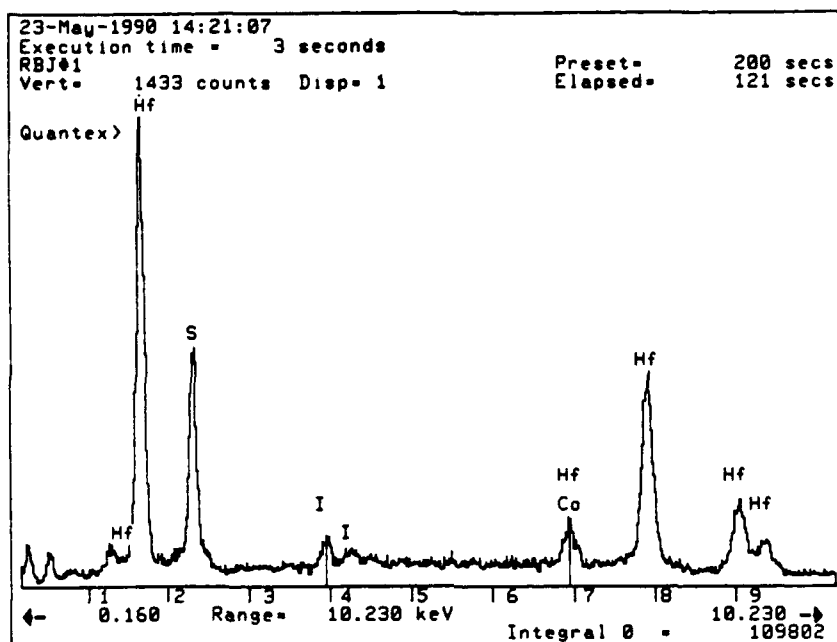


Figure 19. EDS spectrum of  $\text{HfS}_2$  following cobaltocene intercalation and  $\text{I}_2$  treatment. Both Co and I are present.

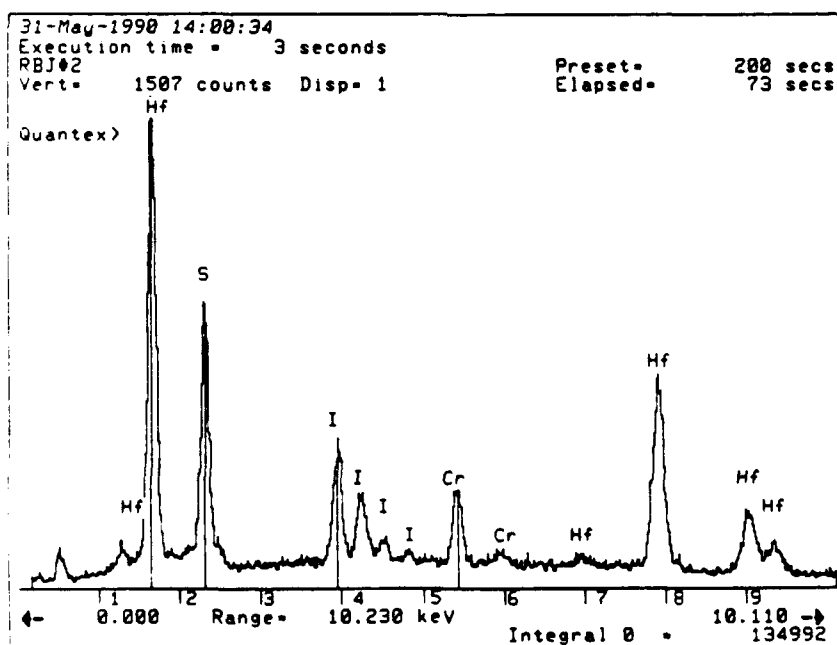


Figure 20. EDS spectrum of  $\text{HfS}_2$  following chromocene intercalation and  $\text{I}_2$  treatment. Both Cr and I are present in significant quantities.

Table 14. Metallocene and I<sub>2</sub> intercalation into HfS<sub>2</sub> single crystal powder.

Cobaltocene and I <sub>2</sub> Intercalation			Chromocene and I <sub>2</sub> Intercalation		
d(Å)	I/I <sub>0</sub>	hkl	d(Å)	I/I <sub>0</sub>	hkl
5.868	100	001	5.868	00	001
3.143	56	100	3.143	18	100
2.772	56	101	2.941	13	002
2.144	27	102	2.772	31	101
1.817	27	110	2.146	25	102
1.734	14	111	1.953	8	003
1.664	12	103	1.817	12	110
1.571	7	--	1.737	9	111
1.519	10	201	1.658	14	103
			1.521	10	201
			1.465	5	004
			1.332	6	104

The presence of iodine in the HfS<sub>2</sub>-metallocene intercalation compound was confirmed by thermogravimetric analysis of HfS<sub>2</sub> crystal-powder. In Figure 21 a comparison is made of the weight loss on heating HfS<sub>2</sub> crystal powder treated with I<sub>2</sub> (vapor phase 300°C for 4 days), chromocene intercalated, and iodine-treated chromocene intercalated material. As expected the iodine treated HfS<sub>2</sub> shows negligible weight loss after heating to 800 °C. There is no intercalation of iodine in as-grown HfS<sub>2</sub> crystal-powder which is confirmed by the absence of a weight change on heating. In addition, it is clear that very little residual iodine remains on the surface of the powder after methanol rinsing. The chromocene intercalated HfS<sub>2</sub> also shows very little weight change on heating, indicating considerable stability of the intercalated guest-host complex. After treatment in iodine, however, the chromocene-intercalated HfS<sub>2</sub> exhibits a 22% weight loss on heating to 800°C. The weight loss must be due to volatilization of I<sub>2</sub> or a chromocene-I<sub>2</sub> complex from the van der Waals' gap. Since the weight loss begins at low temperatures (<100°C) and gradually increases throughout the heating period, sublimation of an intercalated species is suggested. The large amount of intercalated iodine indicated by the 22% weight loss is also supported by the relatively intense iodine peaks in the EDS spectra (Figure 20). Although the data provide strong evidence for "intercalation" of iodine in chromocene intercalated HfS<sub>2</sub>, the nature and extent of the interaction between I<sub>2</sub> and the HfS<sub>2</sub> or chromocene could not be determined from the experiments described. In particular, the degree of electronic charge transfer between the guest iodine and the ionized chromocene could not be measured and the question of whether an I<sub>2</sub>-chromocene charge transfer complex is formed remains unanswered.

The situation with cobaltocene intercalated HfS<sub>2</sub> was considerably different due to the comparatively poor thermal stability of the cobaltocene intercalate. Figures 22 and 23 show TGA data for HfS<sub>2</sub> intercalated for 3 and 5 days, respectively, with cobaltocene and then treated with I<sub>2</sub> at 300°C. The cobaltocene intercalate appears to be unstable at temperatures over ~200°C and some cobaltocene may have decomposed or deintercalated from the HfS<sub>2</sub> during iodine treatment. For both the 3 and 5 day samples, a small additional weight loss was observed with the I<sub>2</sub> treated samples, indicating some "intercalation." The instability of the cobaltocene I<sub>2</sub> intercalant is reflected in the comparatively low intensity of the Co and I peaks in the EDS spectrum (Figure 19).

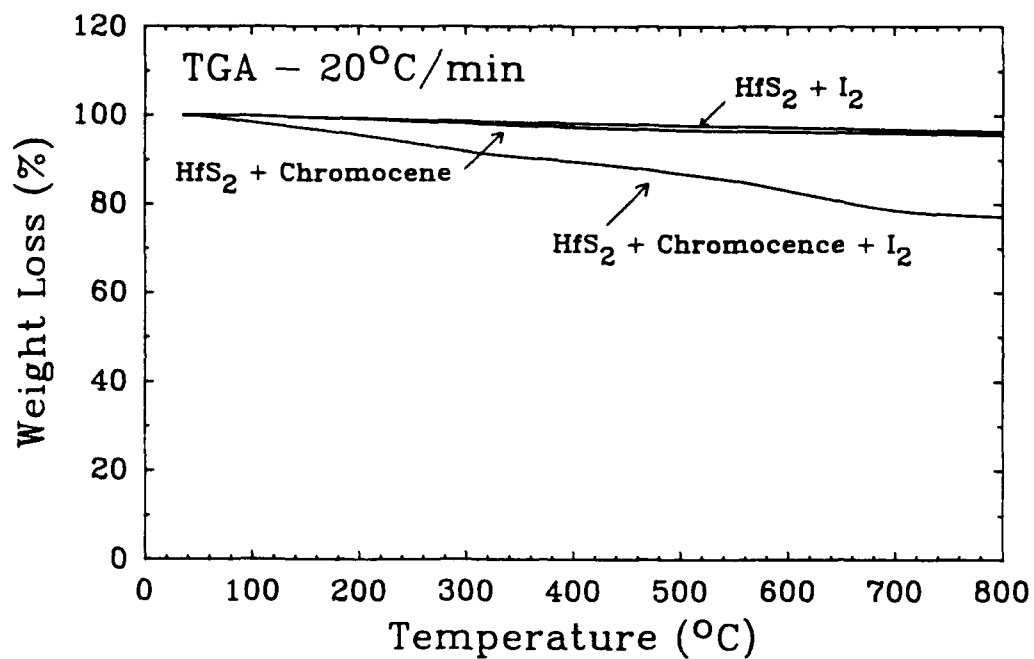


Figure 21. TGA spectrum of chromocene intercalated  $\text{HfS}_2$  following heat treatment in  $\text{I}_2$ .

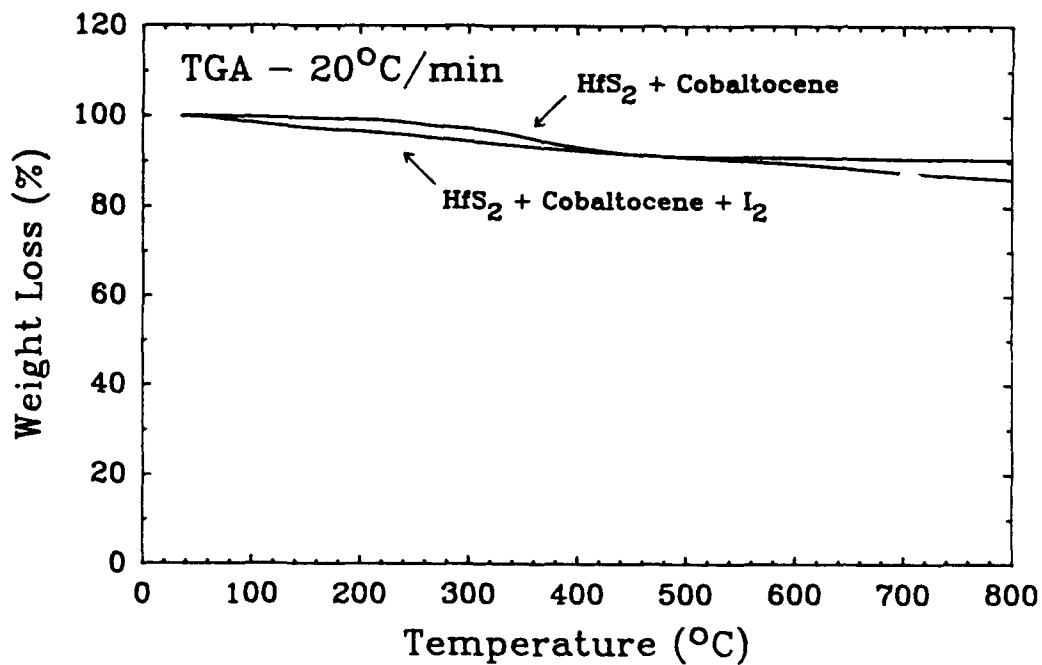


Figure 22. TGA spectrum of cobaltocene intercalated  $\text{HfS}_2$  (3 days at 300°C) following heat treatment in  $\text{I}_2$ .

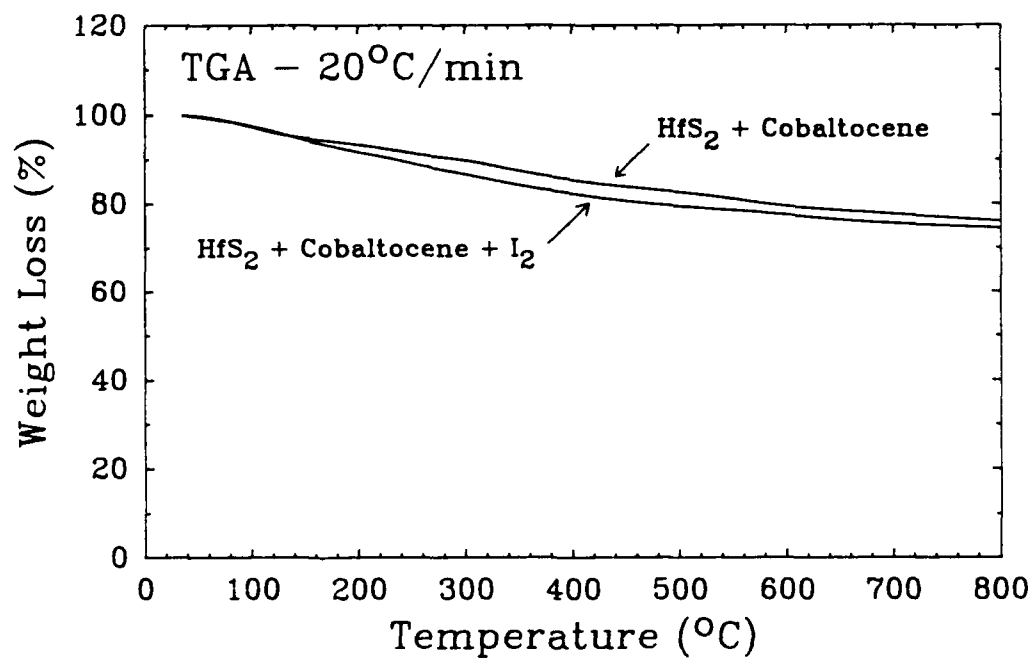


Figure 23. TGA spectrum of cobaltocene intercalated  $\text{HfS}_2$  (5 days at  $300^\circ\text{C}$ ) following heat treatment in  $\text{I}_2$ .

## SECTION 7

### CONCLUSION

A large and reversible IR reflectance modulation is possible with alkali metal intercalated  $\text{HfS}_2$  and  $\text{ZrS}_2$ . A reflectance modulation of 0.01% to 50% (optical density range of 4.0 to 0.3) in the 2-16  $\mu\text{m}$  wavelength range was demonstrated for a  $\text{Li}_x\text{HfS}_2$  crystal chemically lithiated with n-butyllithium and delithiated with iodine. A similar, although less dramatic, optical modulation was observed with  $\text{Ag}_x\text{HfS}_2$ . The smaller absorbance range observed with the Ag intercalate is due to the lower initial Ag concentration and incomplete deintercalation with iodine. To translate this large and broadband IR modulation into a practical optical switching device required the formation of an electron donor-acceptor complex in the van der Waals' gaps of the crystals. Electron donor intercalation is readily achieved because of coulombic stabilization of the intercalated crystal through the interaction of the electronegative chalcogens (i.e., S atoms) adjacent to the van der Waals' gaps and the cation of the intercalated donor.

It is apparent from the results of the Phase II program that the intercalation of an electron acceptor into group IV dichalcogenide crystals is energetically unfavorable and often accompanied by physical exfoliation and destruction of the crystal. Iodine is effective in deintercalating alkali or alkali-like metals from  $\text{HfS}_2$  and  $\text{ZrS}_2$  and no intercalation reaction to form  $\text{LiI}$  or  $\text{AgI}$  charge-transfer complexes in the van der Waals' gaps of the crystals was identified. To overcome this problem, mixed-metal (group IV and V) dichalcogenide crystals, that are intrinsically doped n-type, were grown by the CTVT process. These crystals had higher electrical conductivities and were more IR reflective than  $\text{HfS}_2$  crystals, however, attempts to intercalate iodine into the mixed-metal crystals produced extensive exfoliation. The large size of the iodine acceptor suggested the need to expand the van der Waals' gap prior to  $\text{I}_2$  intercalation. The use of metallocenes, principally chromocene, to create a 5 Å expansion of the van der Waals' gap of  $\text{HfS}_2$  was successful and led to the preparation of  $\text{I}_2$  "intercalated" chromocene- $\text{HfS}_2$ . The nature of the bonding between the intercalated  $\text{I}_2$  and both the chromocene and  $\text{HfS}_2$  remains unknown.

Electrically driven optical switching in the 700-1100 nm range was observed in  $\text{HfS}_2$  crystals that had been lithiated and treated in iodine. A sharp increase in electrical conductivity and decrease in transmittance was observed at electrical field strengths of approximately 0.7 V/ $\mu\text{m}$  in the c-axis direction. The observed switching was fully reversible and did not depend on the polarity of the applied voltage. This current-voltage behavior of the switching in intercalated crystals was different from that reported for "electroformed"  $\text{SnS}_2$  or  $\text{HfS}_2$  (7,10-12).

The major difficulty encountered in the Phase II program was the unsuitability of the dichalcogenide crystals as hosts for electron acceptors even in the presence of intercalated electron donors or in crystals grown directly with mixed group IV and V metals. The use of bulky electron donors to increase the van der Waals' spacing was successful in promoting some form of iodine intercalation but the electrical and optical characteristics of these crystals remain to be determined. Besides the dichalcogenides, other layered materials that are amphoteric (have both acid and base properties) and intercalate both electron donors or acceptors directly would have potential as a guest for electron donor-acceptor complexes. Graphite is the best example of such a material (13).

## SECTION 8

### LIST OF REFERENCES

1. H. Schafer, "Chemical Transport as a Preparative Procedure," in *Preparative Methods in Solid State Chemistry*, P. Hagenmuller ed. (New York: Academic Press, 1972), pp. 251-277.
2. D.L. Greenway and R. Nitsche, "Preparation and Optical Properties of Group IV-VI<sub>2</sub> Chalcogenides Having the CdI<sub>2</sub> Structure," *J. Phys. Chem. Solids*, **26**, 1445 (1965).
3. M.S. Whittingham, "Chemistry of Intercalation Compounds: Metal Guests in Chalcogenide Hosts," *Prog. Solid State Chem.* **12**, 41 (1978).
4. M.G. Bell and W.Y. Liang, *Adv. Phys.* **18**, 53 (1976).
5. L.J. van der Pauw, *Phillips Res. Repts.* **13**, 1 (1958).
6. H.H. Wieder, *Laboratory Notes on Electrical and Galvanomagnetic Measurements* (New York: Elsevier Scientific Publishing Company, 1979).
7. S. Ahmed and P.A. Lee, "Electrical properties and memory effects in hafnium disulphide single-crystal devices," *J. Phys. D: Appl. Phys.*, **6** 593 (1973)
8. M.B. Dines, "Intercalation of Metallocenes in the Layered Transition-Metal Dichalcogenides," *Science*, **188**, 1210 (1975).
9. T.R. Bera, D. Sen and R. Ghosh, "Charge Transfer Adducts of Metal Complexes of Pi-Donor Ligands with I<sub>2</sub> and TCNQ," *Spectrochimica Acta*, **45A**, 985 (1989).
10. P.A. Lee, G. Said, and R. Davis, "Negative Resistance and switching Effect in the Single Crystal Layer Compounds SnS<sub>2</sub> and ZrS<sub>2</sub>," *Solid State Commun.* **7**, 1359 (1969).
11. G. Said and P.A. Lee, "Electrical Conduction Mechanisms in Tin Disulphide," *Phys. Sta. Sol. (a)* **15**, 99 (1973).
12. S.G. Patil and R.H. Tredgold, "Electrical and Photoconductive Properties of SnS<sub>2</sub> Crystals," *J. Phys. D: Appl. Phys.* **4**, 718 (1971).
13. M.S. Dresselhaus, "Intercalation in Layered Materials," *MRS Bulletin*, March 1987, p. 25.
14. A.D. Yoffe, "Physical Properties of Intercalated Solids," *Solid State Ionics*, **9&10** 59 (1983).
15. A. Nussbaum and R.A. Phillips, *Contemporary Optics for Scientists and Engineers* (Englewood Cliffs, NJ: Prentice-Hall, Inc., 1976), pp. 191-195.

## APPENDIX A

### OPTICAL CHARACTERIZATION OF SINGLE CRYSTAL $\text{HfS}_2$ AND $\text{ZrS}_2$

#### A.1 INFRARED (2-16 $\mu\text{m}$ ) PROPERTIES OF $\text{ZrS}_2$ AND $\text{HfS}_2$ .

Hemispherical reflectance measurements were made using an integrating sphere attachment for an IBM IR/30 Series Fourier transform infrared spectrophotometer. In Figure 24, the hemispherical reflectance of a 3  $\text{cm}^2$   $\text{ZrS}_2$  crystal is shown. The reflectance is about 0.44 at 3  $\mu\text{m}$  and decreases gradually to about 0.38 at 16  $\mu\text{m}$ . The reflectance is due to the contrast in the refractive indices of the crystal and the air. In the Phase I program, the maximum transmittance of thin  $\text{ZrS}_2$  crystals was about 60%. The reflectance measurements establish that essentially all the intensity that is not transmitted is reflected, i.e., absorption in  $\text{ZrS}_2$  is negligible at these wavelengths.

The theoretical reflectance  $R$  for a thin sheet of a nonabsorbing material in air at normal incidence, averaged through interference maxima, can be calculated using well known methods in optics (15) as:

$$R = \frac{2R'}{1 + R'^2} \quad (\text{A} - 1)$$

where  $R'$  is the reflectance of a single air-crystal interface:

$$R' = \left[ \frac{n - 1}{n + 1} \right]^2 \quad (\text{A} - 2)$$

The refractive index  $n$  of  $\text{ZrS}_2$  at 10  $\mu\text{m}$  is approximately 2.85 (estimated from data in reference (4)). With  $n = 2.85$ , Eq. (A-1) yields a theoretical reflectance of 0.44, which agrees very well with the measured value of 0.42 in Figure 24. In a device application, antireflection coatings can increase the transmittance of the crystal to practically 100% at a given wavelength in the infrared.

The hemispherical reflectance of the largest  $\text{HfS}_2$  crystal was measured in the 2-16  $\mu\text{m}$  region. As shown in Figure 25, the hemispherical reflectance (averaged through interference maxima and minima) ranges from about 0.37 at 2.2  $\mu\text{m}$  to 0.27 at 16  $\mu\text{m}$ .

From an estimated refractive index  $n$  of  $\text{HfS}_2$  at 10  $\mu\text{m}$  (4), the calculated reflectance of  $\text{HfS}_2$  is 0.44. The calculated value is somewhat above the measured value of 0.27. On the other hand, the reflectance rises significantly below 3  $\mu\text{m}$  to a value at 2.5  $\mu\text{m}$  of 0.37, which agrees more closely with the predicted value. The transmittance of the same crystal was also determined in the 2-16  $\mu\text{m}$  region. As shown in Figure 26, the transmittance at 2.5  $\mu\text{m}$  is about 0.58, but decreases with increasing wavelength to around 0.30 above 6  $\mu\text{m}$ . From Figures 25 and 26, the sum of the transmittance and reflectance is nearly unity at 2.5  $\mu\text{m}$ , which indicates that the crystal is essentially nonabsorbing at this wavelength. At a wavelength of 10  $\mu\text{m}$ , however, it is clear that significant absorption occurs in the crystal because the sum of the reflectance and transmittance is only 0.57. The source of the absorption may be shallow donor or acceptor impurities. Absorption in this region of the mid-infrared was not present in all  $\text{HfS}_2$  crystals.

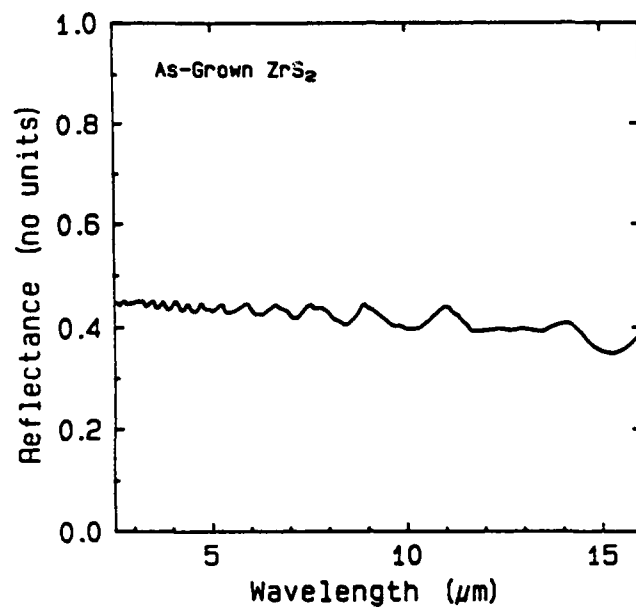


Figure 24. Hemispherical reflectance of an as-grown  $\text{ZrS}_2$  crystal.

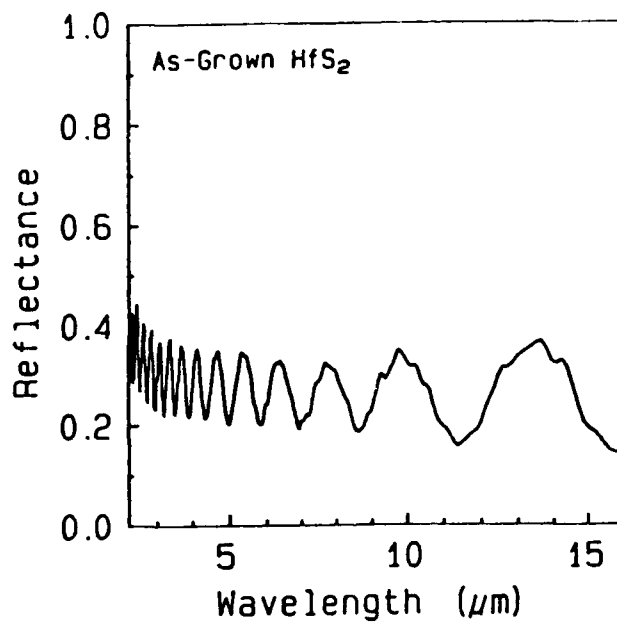


Figure 25. Hemispherical reflectance of an as-grown  $\text{HfS}_2$  single crystal with a thickness of 15  $\mu\text{m}$ .

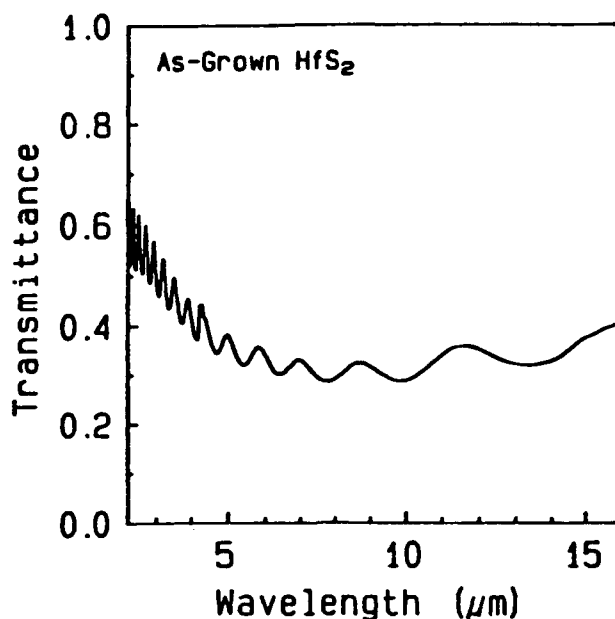


Figure 26. Transmittance of the same  $\text{HfS}_2$  single crystal as in Figure 25.

## A.2 ABSORBANCE OF $\text{ZrS}_2$ AND $\text{HfS}_2$ IN THE NEAR INFRARED DURING LITHIUM INTERCALATION.

In the Phase I program, transmittance measurements in the mid-infrared (2-16  $\mu\text{m}$ ) were performed on  $\text{ZrS}_2$  and  $\text{HfS}_2$  crystals at various stages of Li intercalation from n-butyllithium in hexane. These measurements demonstrated a continuous increase in the reflectance as Li was taken into the crystals. Similar measurements were carried out in the near infrared from 650-1650 nm on  $\text{ZrS}_2$  and  $\text{HfS}_2$  crystals. The measurements were performed on a Cary-14 spectrophotometer with LUSI II electronics upgrade.

Because both the lithiated crystals and the lithiating solution of n-butyllithium in hexane are highly sensitive to water, precautions were taken to obtain the measurement under dry conditions. Samples were prepared by mounting a crystal onto the end of a stiff wire with epoxy. The other end of the wire was pushed through a hole which had been drilled into the cap of an optical cuvette to provide a force fit. The wire supported the crystal in a solution of n-butyllithium in hexane during the measurement. A cuvette was partially filled with n-butyllithium solution under a dry Ar atmosphere in a glove box. For the  $\text{ZrS}_2$  crystal, the concentration of n-butyllithium was 0.22M, while for  $\text{HfS}_2$  it was 0.44M. The support wire was drawn through the cap such that the crystal remained above the solution when the cuvette was capped. After removing the cuvette from the glove box and placing it in the spectrophotometer, the crystal was lowered into the n-butyllithium solution. The reference was a cuvette filled with n-butyllithium solution. Absorbance measurements were obtained at times from <1 min to 5 hr after immersion.

Figure 27 shows the near-infrared absorbance of a 15  $\mu\text{m}$  thick  $\text{HfS}_2$  crystal at selected times after submerging it in the n-butyllithium solution. The absorbance rises first and most rapidly at long wavelengths. At 75 min, the spectrum shows rising absorbance with increasing wavelength through the near infrared. This shape typifies a Drude edge, in which reflection and absorption by

free carriers dominate the long wavelength region of the spectrum. As the concentration of lithium in the crystal increases, the density of free electrons increases as well. This increase causes the Drude edge to sharpen and move to shorter wavelengths. Such behavior is apparent in comparing the 75 min and 135 min spectra. At 240 min, the edge has moved through the near infrared, and the absorbance level recorded corresponds to a nearly background limited instrument reading. Measurements at longer times were essentially identical. Upon completion of the lithiation to the composition  $\text{LiHfS}_2$ , the coloration of the crystal had altered from orange and transmissive to coppery and reflecting. At full lithiation, the Drude edge extends into the visible region, creating the reflective appearance.

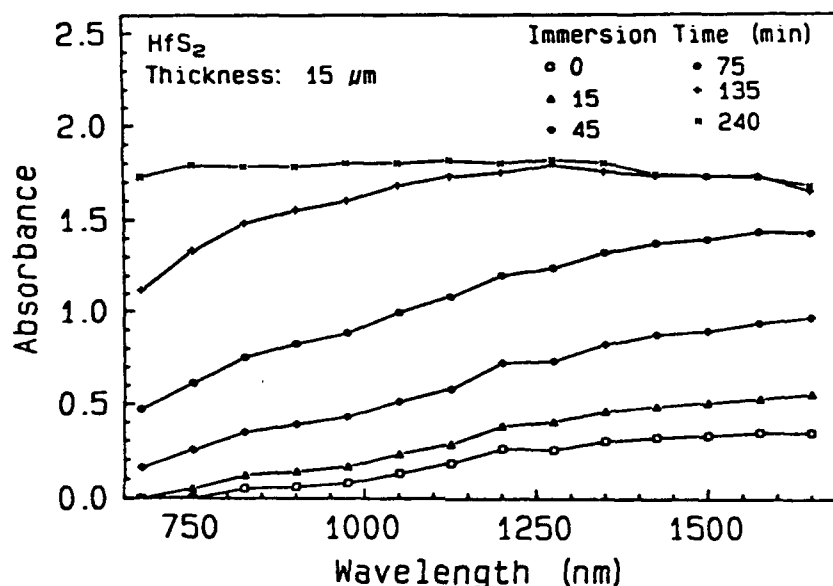


Figure 27. Absorbance spectra in the near infrared of single crystal  $\text{HfS}_2$  during lithium intercalation to the composition  $\text{LiHfS}_2$ . The spectra were recorded after various immersion times in 0.44M n-butyllithium in hexane.

A similar experimental procedure was used to determine the effect of lithiation on the near infrared absorbance of  $\text{ZrS}_2$ . The results in Figure 28 provide an interesting contrast to those in Figure 27 for  $\text{HfS}_2$ . In unlithiated  $\text{ZrS}_2$ , the absorbance rises as the wavelength becomes shorter in the near infrared. The increase in absorbance is due to the increase in absorption associated with the absorption edge in  $\text{ZrS}_2$  at 1.68 eV (740 nm). In  $\text{HfS}_2$ , the absorption edge is at 1.96 eV (630 nm), and it does not affect the measurements in the near infrared. The measurements on  $\text{ZrS}_2$  did not proceed to full lithiation due to experimental difficulties in keeping moisture out of the cuvette for a sufficient period of time. The presence of moisture caused the n-butyllithium solution to become cloudy after several hours, and prevented absorbance measurements from being obtained beyond 180 min. Moisture is also undesirable because it reacts with lithium in the van der Waals' gaps of  $\text{ZrS}_2$  to form  $\text{LiOH}$  on the surface of the crystal. The data in Figure 28 only show the initial stages of lithiation, in which a broadband rise in absorbance occurs. In a highly lithiated crystal, a Drude edge would be expected to develop in the near infrared as it does in  $\text{HfS}_2$ .

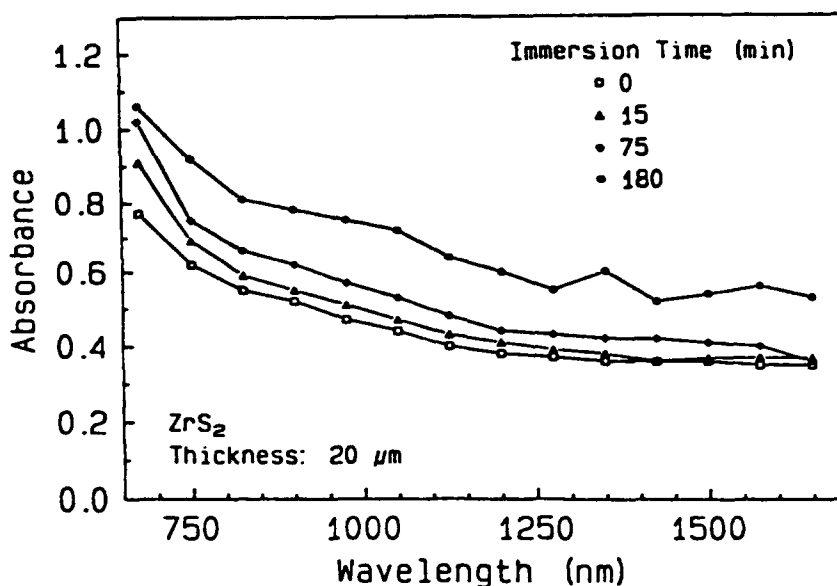


Figure 28. Absorbance spectra in the near infrared of single crystal  $\text{ZrS}_2$  during the initial stages of lithium intercalation (see text). Lithiation was performed by immersing the crystal in 0.22M n-butyllithium in hexane.

From the near infrared absorbance measurements, we conclude that  $\text{HfS}_2$  is capable of providing reflective optical switching throughout the near infrared. At the short wavelength end of the region, a higher free carrier density will be required for switching, which will be more difficult to achieve in practice. On the other hand,  $\text{ZrS}_2$  is not likely to develop a high reflectivity in the short wavelength region of the near infrared due to the presence of the absorption edge.

### VISIBLE (400-700 nm) SPECTRA OF $\text{Li}_x\text{HfS}_2$ SINGLE CRYSTAL.

Figure 29 shows the optical behavior of a  $\text{HfS}_2$  crystal in the visible wavelength region and a small portion of the near infrared upon lithiation in 2.2M n-butyllithium in hexane. The spectra were recorded using a HP 8452 spectrophotometer. Successive spectra show an increase in absorbance due to reflective modulation. For a given intermediate lithium content, the modulation is greater at longer wavelengths. This behavior agrees with that predicted from the Drude model and is a manifestation of an increase in the density of free electrons. At maximum lithiation, corresponding to the composition  $\text{LiHfS}_2$ , the crystal is less than 0.03% transmissive over the entire range of the measurement. Figure A6 also indicates that the wavelength window in which unswitched  $\text{HfS}_2$  is transmissive extends into the red region of the visible spectrum.

### A.3 OPTICAL CHARACTERIZATION OF SINGLE CRYSTAL TIN DISULFIDE.

The hemispherical reflectance and transmittance of an as-grown  $\text{SnS}_2$  crystal was determined from 2-16  $\mu\text{m}$  using an IBM IR/30 Series FTIR spectrometer. Figures 30 and 31 present the results. As discussed in previous quarterly reports in which  $\text{ZrS}_2$  and  $\text{HfS}_2$  were characterized, the reflectance arises from the refractive index contrast between the crystal faces and the surrounding air.

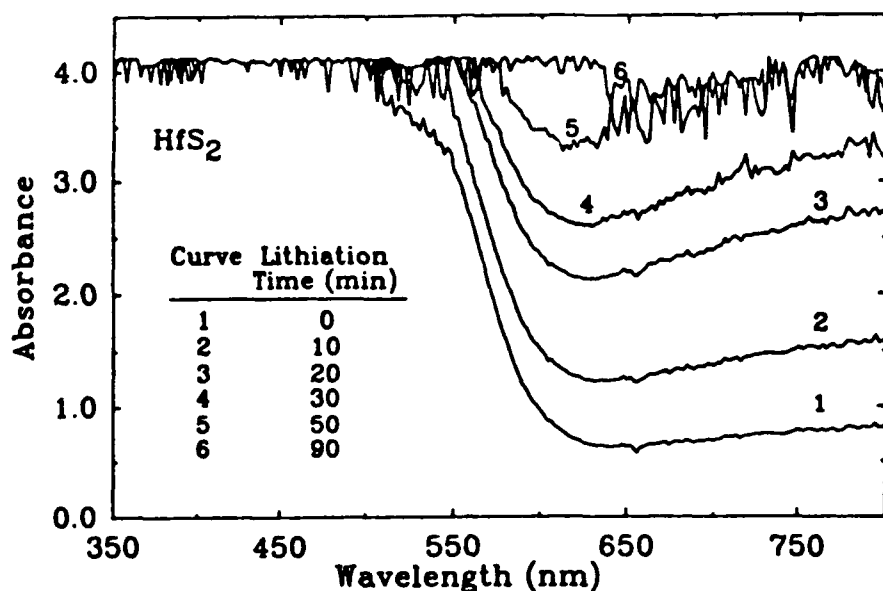


Figure 29. Absorbance of a  $\text{HfS}_2$  single crystal from 350-800 nm during immersion in 2.2M n-butyllithium in hexane. Free electron effects produce a large absorbance increase at wavelengths longer than the optical gap.

The calculated reflectance of  $\text{SnS}_2$  at 10  $\mu\text{m}$ , based on a refractive index of 2.70 (estimated from Eq. A-1) is 0.40; the corresponding value for the transmittance is 0.60. These values agree reasonably well with the experimental values of 0.47 for the reflectance and 0.65 for the transmittance, obtained from Figures 30 and 31 by averaging through interference maxima and minima. Both the reflectance and the transmittance spectra are featureless across the 2-16  $\mu\text{m}$  region. Absorption appears to be negligible since no absorption bands are present and the reflectance and transmittance values essentially sum to unity (actually more than unity due to the experimental choice of standard measurement materials). The absence of absorption indicates that the crystal does not contain significant numbers of electronic defects in the bandgap due to deviations from stoichiometry or growth faults.

The ability of single crystals of  $\text{SnS}_2$  to intercalate lithium was determined from absorbance measurements in a wavelength range of 350-1650 nm. Spectra were obtained in the as-grown condition and as a function of immersion time in 1.1M n-butyllithium in hexane. Measurements from 350-800 nm employed a HP 8452 diode array spectrophotometer, while those from 675-1650 nm were performed using a Cary-14 double beam spectrophotometer with a LUSI electronics upgrade. Spectra obtained on each instrument are presented in Figures 32 and 33, respectively. The only notable feature in the spectra is the absorption edge in the 510-550 nm region. The spectra after a prolonged exposure to the n-butyllithium solution differ only marginally from those taken immediately after immersion. Intercalation of lithium would be expected to increase the absorbance of  $\text{SnS}_2$  in the near infrared.

The optical results demonstrate that  $\text{SnS}_2$  is transparent in much of the visible wavelength region. However, the absence of a significant increase in the absorbance during treatment with n-butyllithium suggests that the rate of lithium intercalation in n-butyllithium solution is extremely low or nonexistent.

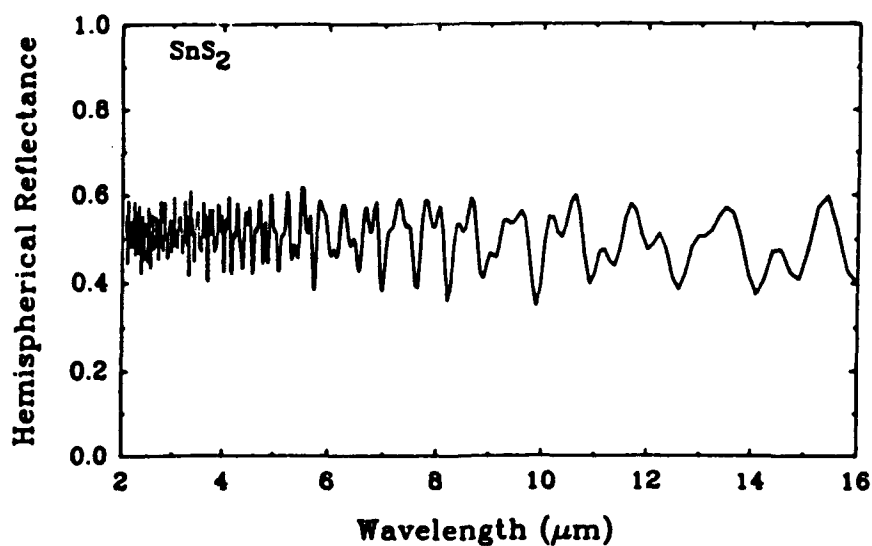


Figure 30. Hemispherical reflectance of an as-grown  $\text{SnS}_2$  crystal from 2-16  $\mu\text{m}$ .

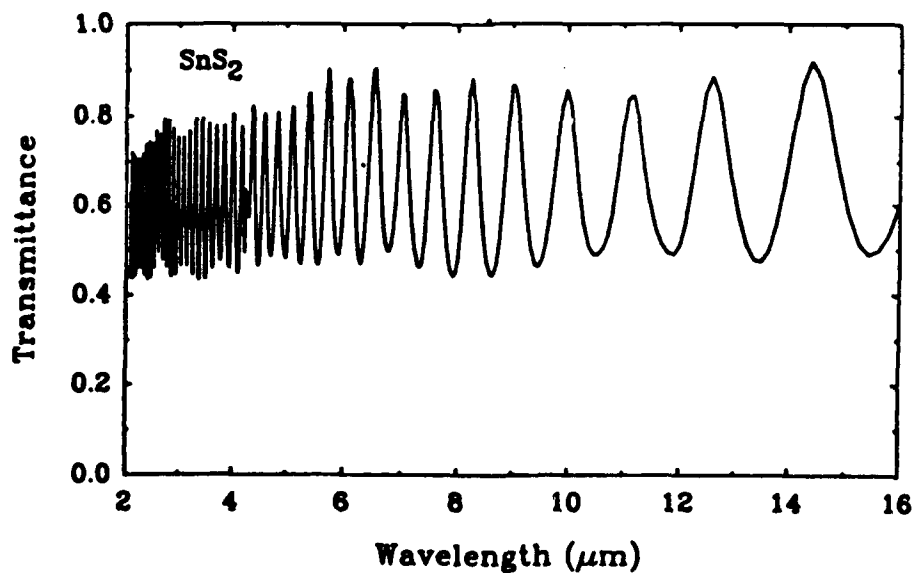


Figure 31. Transmittance of an as-grown  $\text{SnS}_2$  crystal from 2-16  $\mu\text{m}$ .

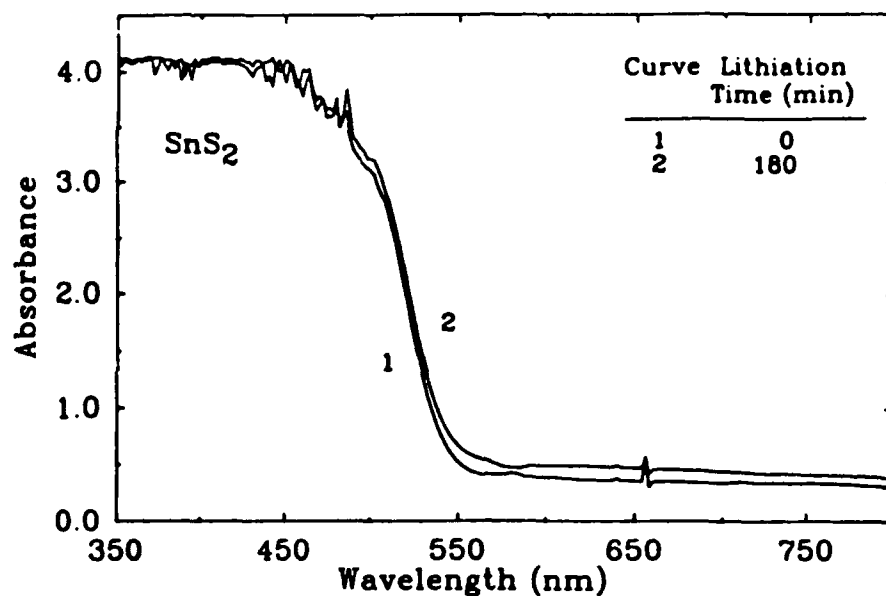


Figure 32. Absorbance of a  $\text{SnS}_2$  single crystal from 350-800 nm during immersion in 1.1M n-butyllithium in hexane. Little or no  $\text{Li}$  intercalation occurred.

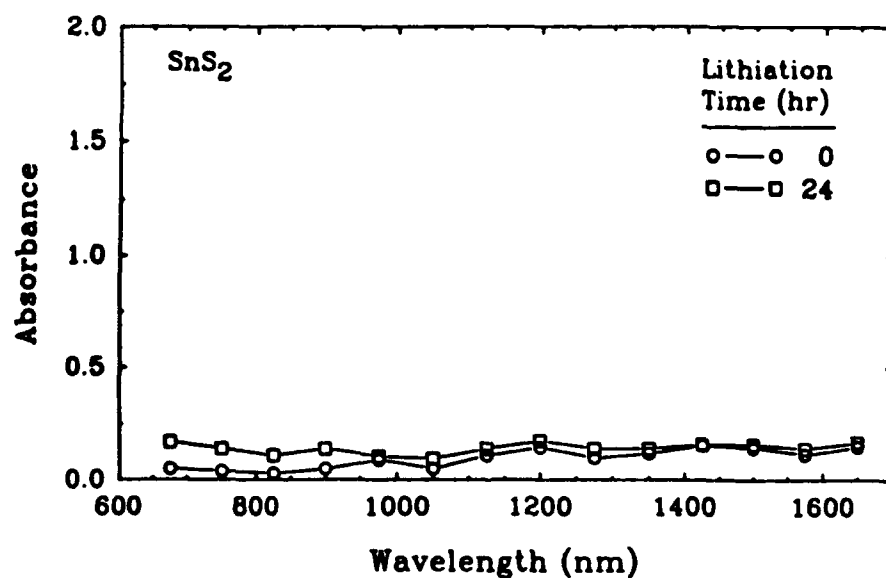


Figure 33. Absorbance of a  $\text{SnS}_2$  single crystal from 675-1650 nm during immersion in 1.1M n-butyllithium in hexane. No evidence of optical effects due to  $\text{Li}$  insertion is present.

## A.5 OPTICAL CHARACTERIZATION OF SINGLE CRYSTAL $\text{CdI}_2$ .

Closed-tube vapor transport grown  $\text{CdI}_2$  single crystals were characterized by infrared transmittance and hemispherical reflectance measurements. The optical measurements indicated highly transparent crystals with a broadband reflectance of 30% in the 2-16  $\mu\text{m}$  wavelength region due to the index mismatch at the air-crystal interface. Attempts to characterize reflectance modulation in  $\text{Li}_x\text{CdI}_2$  were not successful because of decomposition of the  $\text{CdI}_2$  crystal in the n-butyllithium/hexane solution used for lithiation.

As shown in Figures 34 and 35,  $\text{CdI}_2$  has a reflectance of 0.33 at 10  $\mu\text{m}$ , which agrees with the value of 0.29 calculated from Eqs. A-1 and A-2 using  $n = 2.26$  for  $\text{CdI}_2$ . Since the transmittance across the 2-16  $\mu\text{m}$  range is approximately 0.53, the measurements suggest that the absorptance of the crystal is in the neighborhood of 0.14. This absorption is most likely due to a deviation from stoichiometry in the crystal which creates the relative amounts of Cd and I in the starting material for the crystal growth and thereby reduce the infrared absorption.

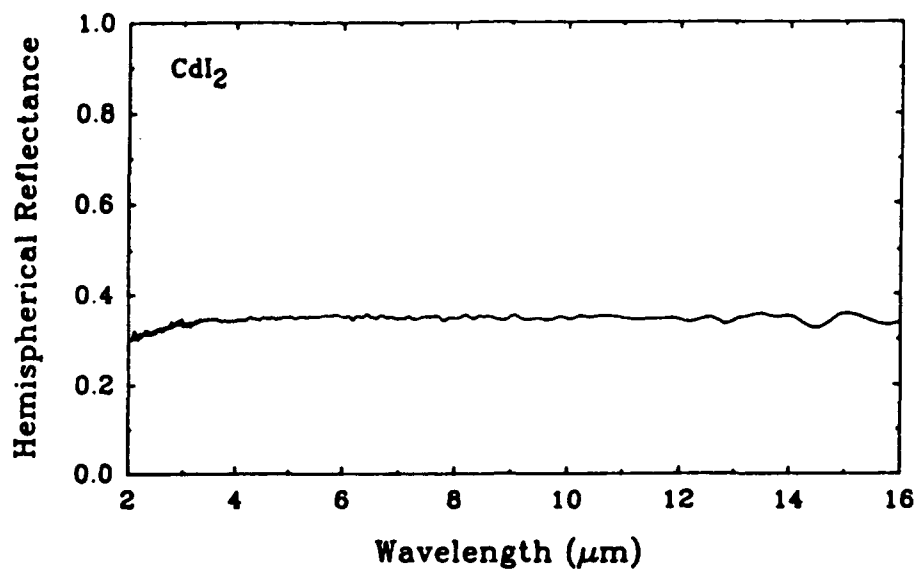


Figure 34. Hemispherical reflectance of an as-grown CdI<sub>2</sub> crystal from 2-16 μm.

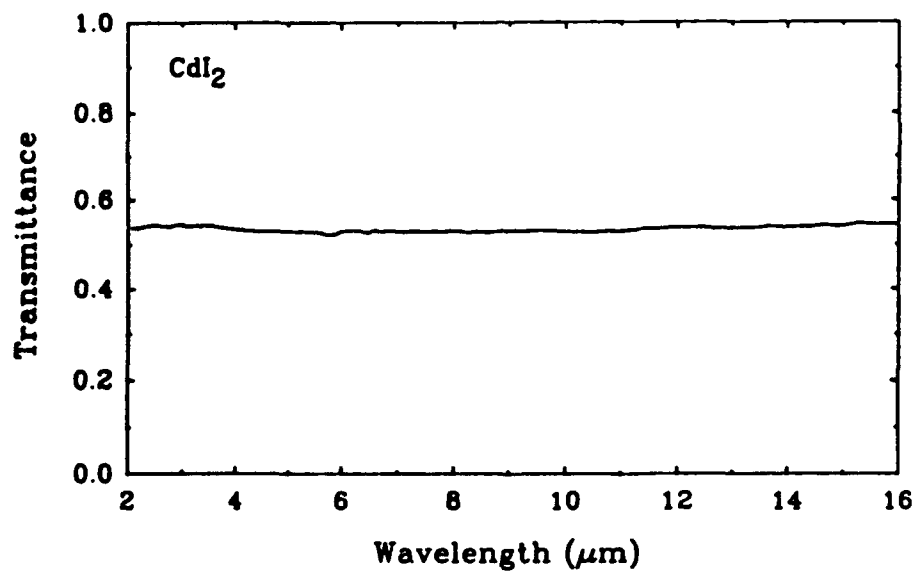


Figure 35. Transmittance of an as-grown CdI<sub>2</sub> crystal from 2-16 μm.

## APPENDIX B

### ORGANIC BASE INTERCALATION

#### ALKYL AMINE INTERCALATION.

To facilitate the intercalation of redox couples (charge-transfer complexes) into the van der Waals' gap of the dichalcogenide crystals, the gap was pre-expanded by intercalation of strongly basic electron donor molecules such as the alkyl amines. In general, amines are readily intercalated in chalcogenides and are weakly bound to the structure inside the gap. Lattice expansion of as much as 56 Å has been reported with the intercalation of n-octadecylamine (14). Pre-expansion of the van der Waals' gap is intended to allow redox couples guest species, electron acceptors in particular, to diffuse more rapidly in the host lattice.

Ethylenediamine (Aldrich Chemical) was used as the intercalant to expand the lattice of  $\text{ZrS}_2$  in the c direction. The intercalation experiments were performed with pure ethylenediamine and a 50% aqueous ethylenediamine solution. The intercalation reaction was allowed to proceed at 75°C for 5 days. The resulting products were then filtered, thoroughly washed with acetone and air dried.

The FTIR spectrum of the collected powder showed an N-H vibration at 6.4  $\mu\text{m}$ , a C-H vibration at 6.8  $\mu\text{m}$ , and a C-N stretching vibration at 9  $\mu\text{m}$ , confirming the presence of ethylenediamine in the  $\text{ZrS}_2$  powder. X-ray diffraction data of the treated powder revealed a complete change in the structure of the crystal. Only one diffraction peak, corresponding to a d-spacing of 16.2 Å, was observed in the intercalated powder. This lack of crystallinity, as observed by x-ray diffraction, is probably due to a severe distortion of the  $\text{ZrS}_2$  crystal lattice. The ethylenediamine ( $\text{NH}_2\text{-CH}_2\text{-CH}_2\text{-NH}_2$ ) could expand the van der Waals' gap of the host lattice by as much as 12 Å. It is possible, therefore, that a massive intercalation of the ethylenediamine destroys the structure of the  $\text{ZrS}_2$  host powder.

A set of experiments were performed to determine the optimum concentration and conditions for ethylenediamine (EDA) intercalation without damaging the structure of the dichalcogenide.  $\text{HfS}_2$  crystal-powder was used for these experiments rather than commercially available material. The  $\text{HfS}_2$  powder was treated with neat EDA for times varying from 15 minutes to 3 days. At 75°C, the intercalation of EDA is so favorable that only 15 minutes was required to expand the (001) d-spacing from 5.82 Å to 9.6 Å. The color of the powder also change from red-purple to greenish-yellow. Thermogravimetric analysis of EDA intercalated  $\text{HfS}_2$  (4 hours at 75°C), shown in Figure B1, indicated about 30% by weight of the powder was EDA, which corresponds to a composition of  $\text{EDA}_{1.7}\text{HfS}_2$ .

Further work on EDA-intercalated dichalcogenides could not be pursued due to time constraints on the program.

## **DISTRIBUTION LIST**

**DNA-TR-91-99**

### **DEPARTMENT OF DEFENSE**

DEFENSE INTELLIGENCE AGENCY  
ATTN: DB-6

DEFENSE NUCLEAR AGENCY  
2 CYS ATTN: TITL

DEFENSE TECHNICAL INFORMATION CENTER  
ATTN: DTIC/FDAB

STRATEGIC DEFENSE INITIATIVE ORGANIZATION  
ATTN: LT COL H SWENSON  
ATTN: MR CARL NELSON  
ATTN: TNS  
ATTN: TNS CAPT P PALMER

### **DEPARTMENT OF THE ARMY**

U S ARMY STRATEGIC DEFENSE CMD  
ATTN: CSSD-H-V S PROFFITT

### **DEPARTMENT OF THE NAVY**

NAVAL OCEAN SYSTEMS CENTER  
ATTN: CODE 7402-T DR K BROMLEY

NAVAL RESEARCH LABORATORY  
ATTN: CODE 5554 F BARTOLI

OFFICE OF NAVAL RESEARCH  
ATTN: DR MATTHEW WHITE

### **DEPARTMENT OF DEFENSE CONTRACTORS**

EIC LABORATORIES INC  
ATTN: J D WESTWOOD  
ATTN: L L WU  
ATTN: R B JONES  
ATTN: R D RAUH  
ATTN: S F COGAN  
ATTN: T H NGUYEN

KAMAN SCIENCES CORP  
ATTN: DASAC

KAMAN SCIENCES CORPORATION  
ATTN: DASAC